

## Journal Pre-proofs

Novel Scaffold Hopping of Potent Benzothiazole and Isatin Analogues linked to 1,2,3-Triazole Fragment that Mimics Quinazoline Epidermal Growth Factor Receptor Inhibitors: Synthesis, Antitumor and Mechanistic Analyses

Nadjet Rezki, Meshal A. Almeahmadi, Saleh Ihmaid, Ahmed M. Shehata, Abdelsattar M. Omar, Hany E. A. Ahmed, Mohamed Reda Aouad

PII: S0045-2068(20)31430-9  
DOI: <https://doi.org/10.1016/j.bioorg.2020.104133>  
Reference: YBIOO 104133

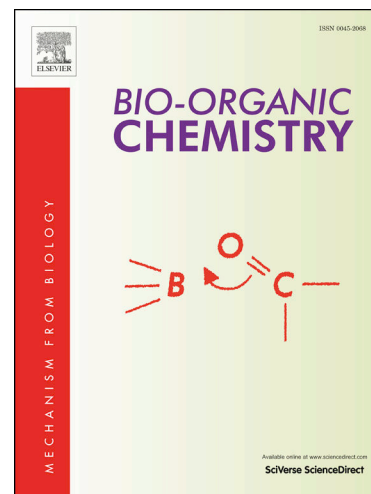
To appear in: *Bioorganic Chemistry*

Received Date: 11 June 2020  
Revised Date: 11 July 2020  
Accepted Date: 18 July 2020

Please cite this article as: N. Rezki, M.A. Almeahmadi, S. Ihmaid, A.M. Shehata, A.M. Omar, H. E. A. Ahmed, M. Reda Aouad, Novel Scaffold Hopping of Potent Benzothiazole and Isatin Analogues linked to 1,2,3-Triazole Fragment that Mimics Quinazoline Epidermal Growth Factor Receptor Inhibitors: Synthesis, Antitumor and Mechanistic Analyses, *Bioorganic Chemistry* (2020), doi: <https://doi.org/10.1016/j.bioorg.2020.104133>

This is a PDF file of an article that has undergone enhancements after acceptance, such as the addition of a cover page and metadata, and formatting for readability, but it is not yet the definitive version of record. This version will undergo additional copyediting, typesetting and review before it is published in its final form, but we are providing this version to give early visibility of the article. Please note that, during the production process, errors may be discovered which could affect the content, and all legal disclaimers that apply to the journal pertain.

© 2020 Elsevier Inc. All rights reserved.



# Novel Scaffold Hopping of Potent Benzothiazole and Isatin Analogues linked to 1,2,3-Triazole Fragment that Mimics Quinazoline Epidermal Growth Factor Receptor Inhibitors: Synthesis, Antitumor and Mechanistic Analyses

Nadjet Rezki,<sup>1,\*</sup> Meshal A. Almeahmadi,<sup>1</sup> Saleh Ihmaid,<sup>2</sup> Ahmed M. Shehata,<sup>3,4</sup> Abdelsattar M. Omar,<sup>5,6</sup> Hany E. A. Ahmed,<sup>2,7\*</sup> Mohamed Reda Aouad<sup>1</sup>

Journal Pre-proofs

<sup>1</sup>Department of Chemistry, College of Science, Taibah University, Al-Madinah Al-Munawarah 30002, Saudi Arabia

<sup>2</sup>Pharmacognosy and Pharmaceutical Chemistry Department, College of Pharmacy, Taibah University, Al-Madinah Al-Munawarah, Saudi Arabia

<sup>3</sup>Pharmacology and Toxicology Department, College of Pharmacy, Taibah University, Al-Madinah Al-Munawarah, Saudi Arabia.

<sup>4</sup>Department of Pharmacology and Toxicology, Faculty of Pharmacy, Beni-Suef University, Egypt.

<sup>5</sup>Pharmaceutical Chemistry Department, Faculty of Pharmacy, King Abdulaziz University, Jeddah 21589, Saudi Arabia

<sup>6</sup>Pharmaceutical Chemistry Department, Faculty of Pharmacy, Al-Azhar University, Nasr City 11884, Cairo, Egypt

<sup>7</sup>Pharmaceutical Organic Chemistry Department, Faculty of Pharmacy, Al-Azhar University, 11884 Nasr City, Cairo, Egypt

\*Corresponding author

E-mail address: [nadjetrezki@yahoo.fr](mailto:nadjetrezki@yahoo.fr), [heahmad@taibahu.edu.sa](mailto:heahmad@taibahu.edu.sa)

## Abstract

A series of benzothiazole/isatin linked to 1,2,3-triazole moiety and terminal sulpha drugs **5a-e** and **6a-e** were synthesized and evaluated for cytotoxic activity against a panel of cancer cell lines. The novel compounds showed variable IC<sub>50</sub> range of activity and some of them were potent compared to reference drug. The promising compounds were subjected as postulated the mimicry proposal for quinazoline-based EGFR inhibitors for their inhibitory profile against EGFR TK enzyme. That data obtained revealed that most of these compounds were potent EGFR TK inhibitors at nanomolar concentrations. Among these, compounds **5a** and **5b** showed more potent activity on EGFR compared to erlotinib (IC<sub>50</sub> 103 and 104 versus 67.6 nM). Based upon the results, molecular docking analysis was performed on EGFR receptor and proved the strong contribution of fragments; benzothiazole, isatin, and triazole to the binding ATP pocket. When these selected compounds **5a** and **5b** were tested in an HepG2 model, they could effectively inhibited tumor growth, strongly induced cancer cell apoptosis, and suppressed cell cycle progression leading to DNA fragmentation. Well-DMET profile of the most active derivatives was presented and compared to the reference drugs. Taken together, we introduced novel triazole-sulpha drug hybrid for the first time as EGFR inhibitors and the results of our studies indicate that the newly discovered inhibitors have significant potential for anticancer treatment.

**Keywords:** Triazole; benzothiazole; isatin; EGFR TK; apoptosis; cell cycle analysis; anticancer activity.

**Introduction:**

Cancer is considered as one of the most threatening disease affecting many of populations. WHO reported in 2020, that the incidence of population is 18.1 million cancer cases and mortality about 9.6 million deaths occurred [1]. Over the past decade, different strategies were offered to prevent cancer from developing and stop patients from deteriorating, and lastly, a novel series of selective chemotherapeutic drugs such as enzyme-mediated drugs like imatinib, gefitinib, erlotinib, and afatinib have been launched worldwide for the treatment of cancer [2]. The action targets of these innovative drugs are mainly directed to impact the signal transduction pathway of the epidermal growth factor receptor (EGFR) [3]. The over-expression and/or mutation of EGFR plays an important role in the growth of cancer including cell proliferation, anti-apoptosis, metastasis, and angiogenesis [4-7]. The EGFR has been reported as an attractive target for cancer therapy [8, 9]. Over recent years, many scientists have discovered the mechanism of the EGFR that the binding of specific ligands such as epidermal growth factor (EGF) and transforming growth factor  $\alpha$  (TGF $\alpha$ ) to the extracellular domain of EGFR induces the dimerization, activation of intrinsic kinase activity, and subsequent autophosphorylation of EGFR at multiple residues in the cytoplasmic region, while the downstream signaling proteins including phosphoinositide 3-kinase (PI3-K), Akt, mammalian target of rapamycin (mTOR), Ras, Raf, MEK, and extracellular signal-regulated kinase (ERK) stimulate several signal transduction cascades, leading to DNA synthesis and cell proliferation [10, 11]. As it can obviously influence the proliferation of human cancer cells, and even result in the apoptosis of human cancer cells, the EGFR has become a very luminous target for various antitumor candidates [12, 13].

There are different heteroaromatic cyclic structures representing a core structures for most of marketed drugs [14]. Among these, benzothiazole and isatin, which are considered as promising chemical scaffolds for designing of numerous biologically and pharmacologically active drugs [15-20]. 1,2,3-Triazoles, one of the most fascinating classes of nitrogen containing heterocycles, have the ability to form various non-covalent interactions such as hydrophobic interactions, hydrogen bonds, van der Waals forces and dipole-dipole bonds with different biological targets that possess diverse pharmaceutical properties [21-27]. In addition, triazole-linked drugs were introduced as novel panel in medicinal chemistry for discovery of potent anticancer agents [28]. The triazole-based drugs exhibited ideal features as metabolically stable bioisosteres of trans-amide bonds and the 1,2,3-triazoles mimic amide bonds in terms of planarity, size, dipolar moment, and hydrogen bonding features [29-31]. Kumbhare et al. introduced novel compounds formed of triazoles and isoxazoles linked 2-phenyl benzothiazole as potential anticancer agents [32]. In the previous work, we introduced a novel scaffold consisting of benzothiazole-linked to triazole derivatives that offering anticancer activity [25, 33-35]. These trials have motivated us to optimize these rationales and changed scaffold based upon the hybridization of hetroaromatic cyclic scaffold linked to the triazole moiety and terminal side chain polar sulphonamides to improve physical properties and confer a favorable pharmacokinetic profile in animals and humans, **Fig. 1**. According to scaffold-hopping strategy [36, 37], the quinazoline fragment of gefitinib was replaced by triazole core structure with methylene linker to benzothiazole/isatin ring as pharmacodynamic group as aniline fragment and ending with polar sulphonamide part. This molecular replacement strategy affords more metabolic stability and hydrogen bonding features for the novel analogs. Moreover, to gain an understanding of the interactions between these novel derivatives and EGFR, hereinafter docking studies are also presented.



The electrostatic potential of all compounds; reference drugs and proposed ligands are displayed with different energy levels (in kcal/mol) of the hydrophobic (green zones), H-bond acceptor (red zones), and H-bond donor (blue zones) maps. Actually, it appears that the comparison of the patterns from **Fig. 3** reveals the molecular features controlling the inhibitory activity are trapped in the properties of the active fragments contributing in the interaction patterns. These fragments vary from the core scaffold to terminal hydrophilic parts as electron-acceptor rich parts and this quite clear in the analysis of the electrostatic potential maps of reference drugs (**Fig. A-B**); red zones. This pattern looks like the electrostatic maps of the target scaffolds as they are rich in electron-acceptors properties and consistent with the other hydrophilic H-donors and neutral properties (**Fig. C-D**).

Journal Pre-proofs

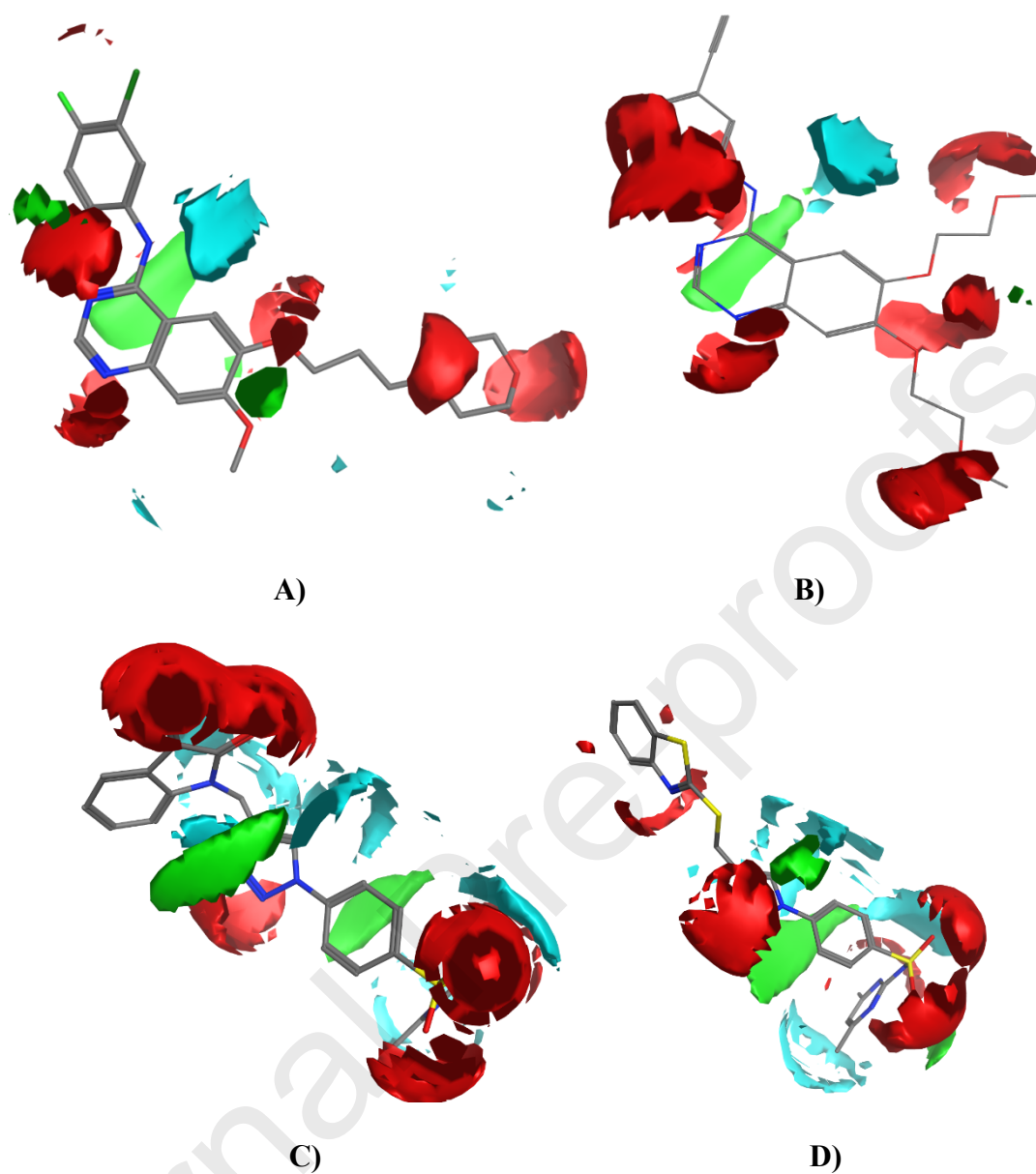


**Fig.2.** Electrostatic map distribution of selected quinazoline-based EGFR TK inhibitors mapped with proposed benzothiazole and isatin-triazole scaffolds.

### 2.1.2. EGFR pocket mapping

X-ray structure of EGFR is shown in (**Fig. 2A**) indicated that 4-anilinoquinazoline erlotinib causes inhibition through binding to the site occupied by ATP during phosphotransfer. The N1 of the quinazoline accepts an H-bond from the Met769 amide nitrogen. We find Thr766, Lys721, and Leu764 are 4 Å from the acetylene moiety on the anilino ring (Thr766 and Leu764 are >3.4 Å). Both Met742 and Cys751 have been suggested to contact inhibitors very similar to erlotinib, but contact distances seen here for both are greater than 4.5 Å. This map of interactions are derived from the analyses of both crystal structures was consistent with previous findings [38, 39].

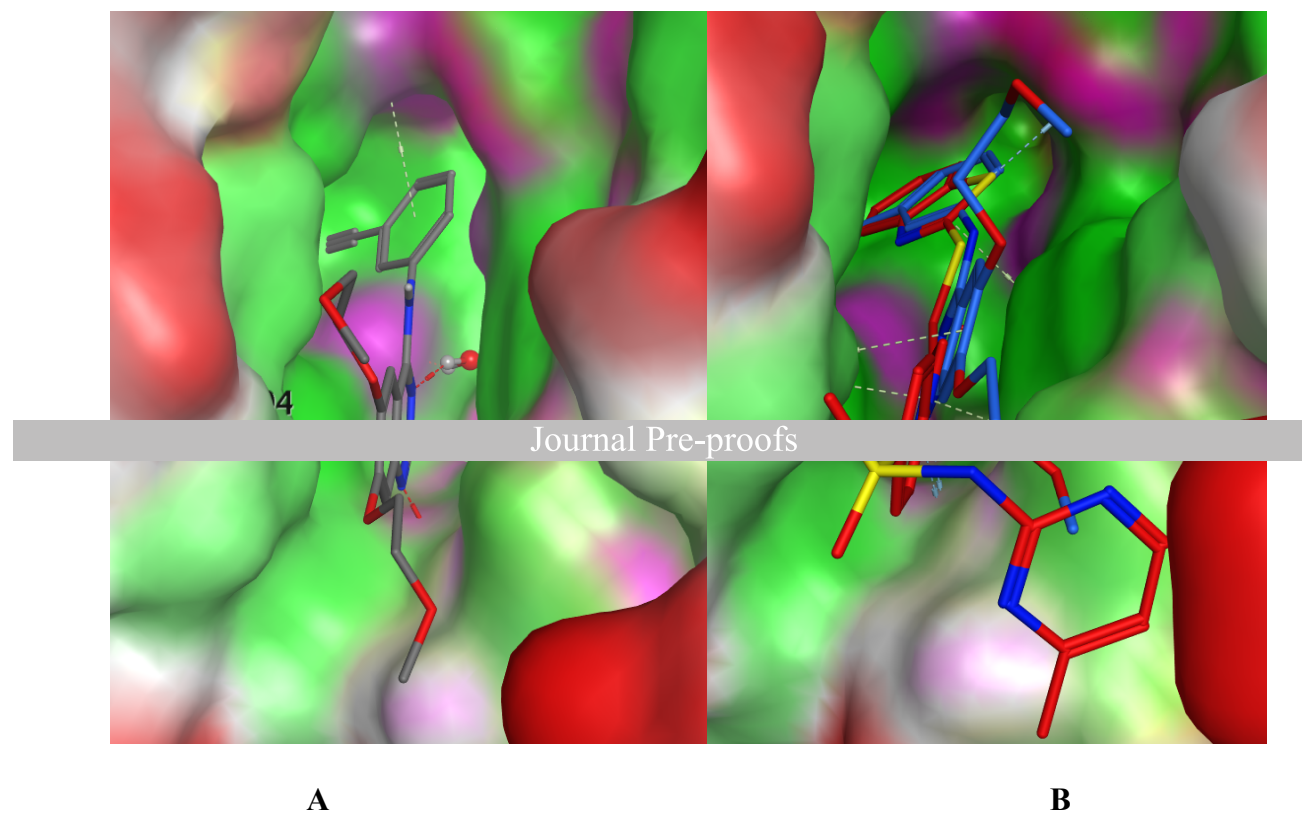


**Fig. 3.** X-ray structures of **A)** EGFR TK with bound erlotinib inhibitor, and **B)** EGFR TK with bound inhibitor erlotinib aligned with proposed benzothiazole-triazole scaffold.

On the basis of the observed interaction patterns and bound inhibitors, we carried out an alignment step of proposed scaffolds to the reference erlotinib ligand in the ATP-pocket and feature mapping were analyzed using the Molecular Operating Environment (MOE) [40] and further refined the alignment through intra- and inter-molecular energy minimization. Based on these alignments; triazole mimics quinazoline, sulphonamide mimics hydrophilic part, and benzothiazole or isatin mimics the fluorenyl moiety (**Fig. 3A**). The model represented substructures of inhibitors that formed characteristic interactions or occupied a hydrophobic pocket within the active site and were considered important for inhibitory activity.

Guided by our structure-based EGFR analysis and comparison of the new proposed scaffold to quinazoline-based inhibitors, we then designed different triazole-based compounds and examined their detailed fit to the EGFR PDB model, which represented the central part of our structure-based design exercise. The novel compounds derived on the basis of a newly proposed triazole-sulphonamide scaffold yielded an excellent fit to binding pocket, as illustrated in (**Fig. 3B**). In exemplary compound, the triazole moiety mapped to quinazoline binding site represented by the donor/acceptor feature. The excellent fit of the newly designed 2-aminothiazole-based compounds to the ATP active site motivated us to synthesize these compounds and test them for anticancer activity targeting the EGFR TK. In this study, a series of 1,2,3 triazoles with sulphonamide side chain were designed and synthesized. Next, their inhibitory potencies of EGFR kinase activity were compared to erlotinib *in vitro*.

## 2.2. Organic synthesis

The synthetic route to the target 1,2,3-triazoles **5a-e** and **6a-e** was performed by the click 1,3-dipolar cycloaddition reaction of the appropriate benzothiazole and/or isatin based alkyne with several sulfa drug azides as depicted in Scheme 1. Thus, we began our investigation by the conversion of sulfadrug amines **1a-e** namely sulfamethazine, sulfadiazine, sulfapyridine, sulfathiazole and sulfaguanidine into their corresponding azides **2a-e**, respectively; *via* diazotization *in situ* catalyzed by sodium nitrite in HCl followed by treatment with sodium azide according to reported procedure [41]. On the other hand, 2-mercaptobenzothiazole and/or isatin on being alkylated with propargyl bromide [34], resulted in the formation of the propargylated benzothiazole **3** and the propargylated isatin **4** in 91 % and 95 % yields, respectively.

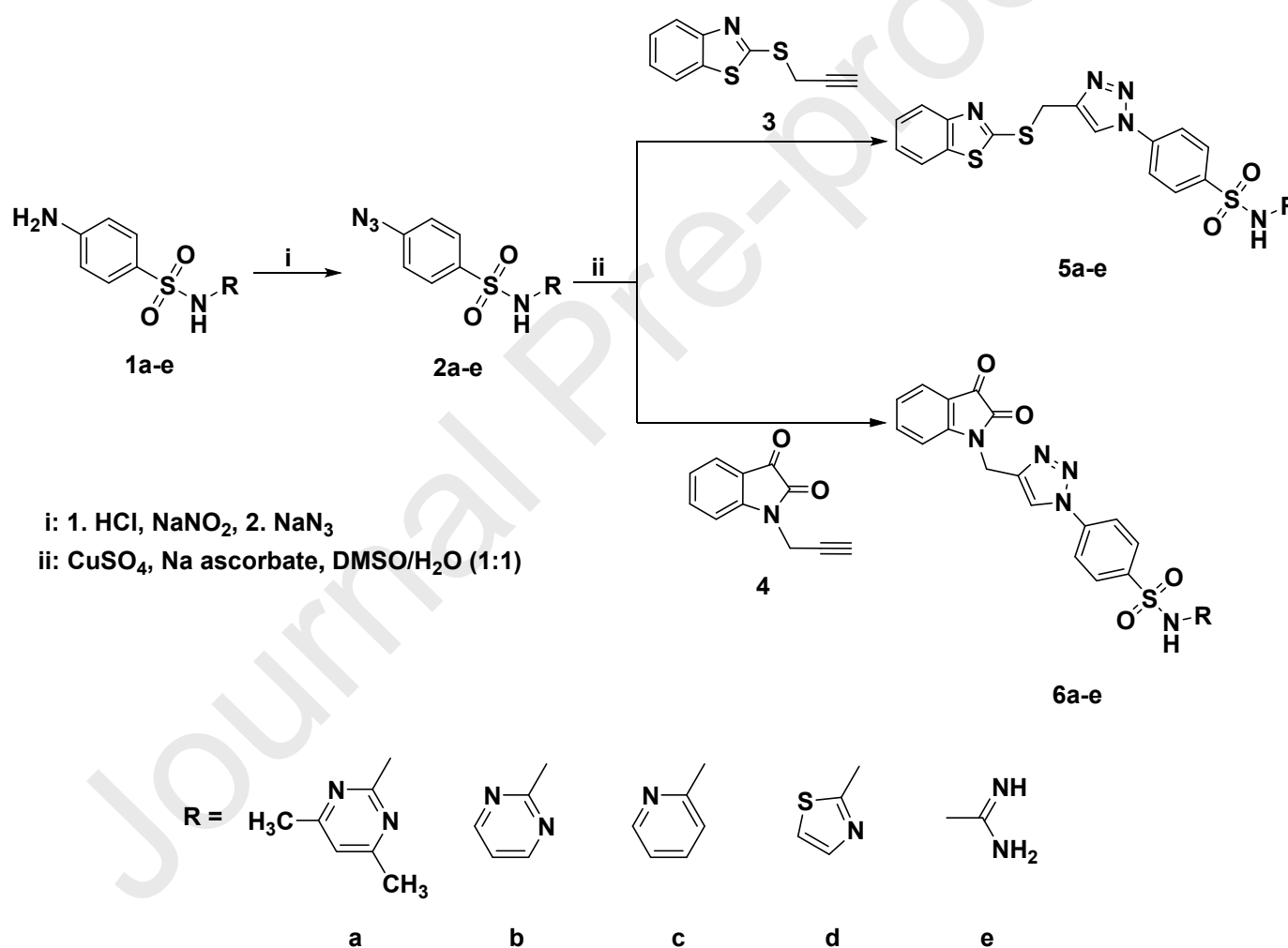
Click 1,3-dipolar cycloaddition reaction of the freshly prepared sulfa drug azides **2a-e** to a stirring solution of 2-(prop-2-yn-1-ylthio)benzo[*d*]thiazole (**3**), copper sulfate and sodium ascorbate; in a mixture of DMSO:H<sub>2</sub>O (1:1) at room temperature for 8-12 h; led to the formation of new 1,2,3-triazole derivatives tethering benzothiazole-sulfa drug molecular conjugates in 84-90 % yields.

The structures of the newly synthesized 1,2,3-triazole-benzothiazole conjugates **5a-e** have been fully characterized by IR, NMR and elemental analysis. The IR spectra showed clearly the disappearance of the alkyne groups of the precursor propargylated **3**, and revealed absorption bands in obvious of

their proposed structures (See experimental section). The formation of the resulted triazoles **5a-e** was also evidences by their  $^1\text{H}$  NMR spectra, which revealed the absence of the terminal acetylenic proton ( $\equiv\text{C-H}$ ) confirming its involvement in the cycloaddition reaction. The spectra also exhibited diagnostic singlets around  $\delta_{\text{H}}$  8.91-8.93 ppm attributed to the aromatic  $\text{CH}$ -triazolyl ring. In addition, the  $\text{SCH}_2$  and  $\text{NH}$  protons were resonated as two singlets at  $\delta_{\text{H}}$  4.79-4.81 ppm and  $\delta_{\text{H}}$  12.19-12.92 ppm, respectively. The  $^{13}\text{C}$  NMR spectra also confirmed the success of the click reactions. The absence of the carbons attributed to the alkyne chain and the presence of new signals assigned to  $\text{SCH}_2$  between  $\delta_{\text{C}}$  27.68-27.70 ppm agreed with the proposed triazole structures. Extra aromatic protons and carbons were recorded in the aromatic area and were listed in the experimental section.

Journal Pre-proofs

Application of our optimized Cu(I) catalyzed click reaction conditions to the propargylated isatin **4** afforded the desired isatin-1,2,3-triazole-sulfa drug hybrids **6a-e** in good to excellent yields 86-91 %. The structures of the resulted 1,2,3-triazole based isatin nucleus **6a-e** were elucidated based on their spectroscopic data. Their IR spectra confirmed the involvement of the terminal alkyne group in the cycloaddition reaction due to the disappearance of the corresponding absorption bands ( $\text{C}=\text{C}$  and  $\equiv\text{C-H}$ ). The examination of the  $^1\text{H}$  NMR spectra also revealed the absence of the  $\text{Sp}$  proton and the presence of characteristic singlets at  $\delta_{\text{H}}$  5.08-5.10 and 8.93-8.96 ppm, attributed to the  $\text{NCH}_2$  and 1,2,3-triazolyl ring protons, respectively. The sulfonamide  $\text{NH}$  protons were observed in the downfield around  $\delta_{\text{H}}$  12.02-12.83 ppm. The remaining protons resonated at their usual chemical shift (See experimental section). In addition, the  $^{13}\text{C}$  NMR spectra recorded new aromatic carbons of the triazole and phenyl rings. The  $\text{NCH}_2$  were observed between  $\delta_{\text{C}}$  34.93-35.48 ppm.



**Scheme 1.** Click synthesis of benzothiazole/Isatin-1,2,3-triazole-sulfa drug molecular hybrids **5a-e** and **6a-e**

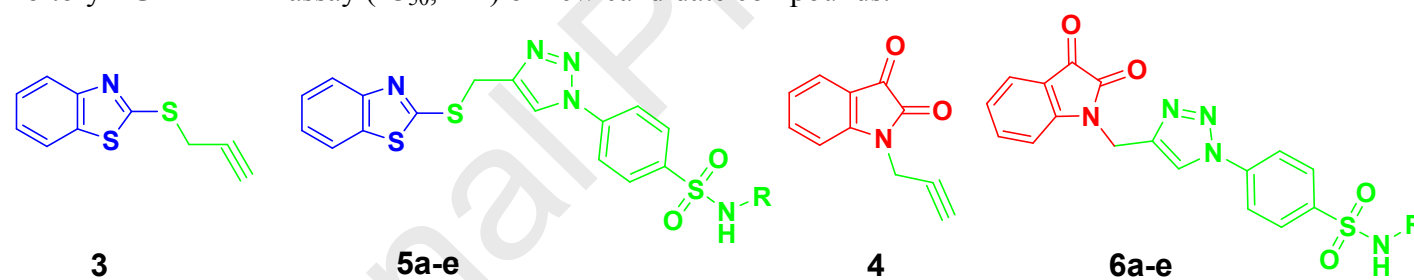
### 2.3. Biological evaluation

#### 2.3.2. EGFR TK inhibitory activity

Based upon the anticancer data, the following mechanism of action can be proposed for benzothiazole/isatin-1,2,3-triazole-sulfa drug hybrids derivatives since their chemical structure, in some respect, resembles benzothiazole/isatin-1,2,3-triazole-sulfa drug hybrids -based EGFR inhibitors which inhibits EGFR tyrosine kinase by binding to the ATP binding site. The epidermal growth factor receptor (EGFR) is considered a cellular trans-membrane tyrosine kinases that is over-expressed in a different types of human tumors (e.g., breast, ovarian, colon, and prostate), their expression levels often correlate with vascularity and is associated with poor prognosis in patients [61]. Thus, the activation process of the EGFR tyrosine kinase and hence activating the anti-apoptotic rap signal transduction cascade is inhibited and the growth of malignant cancer cells is inhibited. The synthesized

benzothiazole/isatin-1,2,3-triazole-sulfa drug hybrids derivatives may be a selective inhibitor of the epidermal growth factor receptor (EGFR) tyrosine kinase over expression through the inhibition of EGFR autophosphorylation and EGF-stimulated signal transduction [62]. However, a detailed receptor study is necessary to reach a concrete conclusion at the close future. Based upon the anticancer screening data, the EGFR enzyme assay was done for all compounds. All results are presented in **Table 1** and assays were done for starting materials and final products. Benzothiazoles showed more inhibitory effect on EGFR target better than isatin ones. The data revealed that derivatives with sulpha substituents of large aromatic rings size are more activity than lower ones and aliphatic side chains. This might be due to the hydrophobic aromatic interactions involved in binding data. The data overall showed that most of the derivatives have potent EGFR inhibition compared to inactive precursors and comparable activity to erlotinib. Among these active derivatives, the **5a** and **5b** analogs with pyrimidine part showed potent nanomolar inhibitory activity, 104-103 nM compared to the reference drug, erlotinib. As already outlined, lipophilicity has been shown in numerous studies to be a general predictor for high P-gp inhibitory potency. This most probably is due to the proposed access path of the compounds, which seems to be directly from the membrane bilayer. On the other hand, high lipophilicity is very often associated with poor oral drug-like properties. This led to the assumption that LogP values between 2 and 3.5 are considered optimal in an oral drug program and prompted Leeson *et al.*, to introduce the concept of lipophilic efficiency (LPE) [42]. LPE is a parameter that combines both potency and lipophilicity and is defined as a measure of how efficiently a ligand exploits its lipophilicity to bind to a given target. Briefly, in a lead optimization series, there is a greater likelihood of achieving good in vivo performance when potency can be increased without increasing logP or logD values. To explore this concept also for EGFR inhibitors, we calculated LPE values for the whole set of target compounds and reference erlotinib drug **Table 1, Fig. 4**. The LogP values vary from -0.4 to 4.4, leading to a lipophilic efficiency range between 6.73 and 1.71. This was done for underlying both relatively good oral absorption and potential for penetration. It was shown that erlotinib has 3.7 LPE and the novel potent derivatives **5a** and **5b** showed less LPE values than it due to somehow the higher LogP values.

**Table 1.** *In vitro* inhibitory EGFR<sup>wild type</sup> assay (IC<sub>50</sub>, nM) of new candidate compounds.



Cpd. ID	IC <sub>50</sub>	LogP	LPE
<b>3</b>	>50000	3.02	3.86
<b>5a</b>	104.29±0.20	4.37	2.61
<b>5b</b>	103.79±1.20	3.76	3.11
<b>5c</b>	254.53±0.82	4.36	2.23
<b>5d</b>	712.29±1.20	4.42	1.72
<b>5e</b>	413.3±0.55	2.13	4.25
<b>4</b>	>25000	0.849	5.691
<b>6a</b>	175.62±0.88	2.20	4.55
<b>6b</b>	290.30±0.82	1.58	4.95
<b>6c</b>	424.20±1.20	2.19	4.18
<b>6d</b>	668.97±1.25	2.25	3.91
<b>6e</b>	468.21±0.82	-0.41	6.73
<b>Erlotinib</b>	76.6±1.20	3.40	3.71

- Data are presented as average IC<sub>50</sub> ± SD (nM) values for at least three experiments. P-value is < 0.05.
- Lipophilic Efficiency was calculated by (LPE = PIC<sub>50</sub> - LogP) equation that is critical for drug likeness.

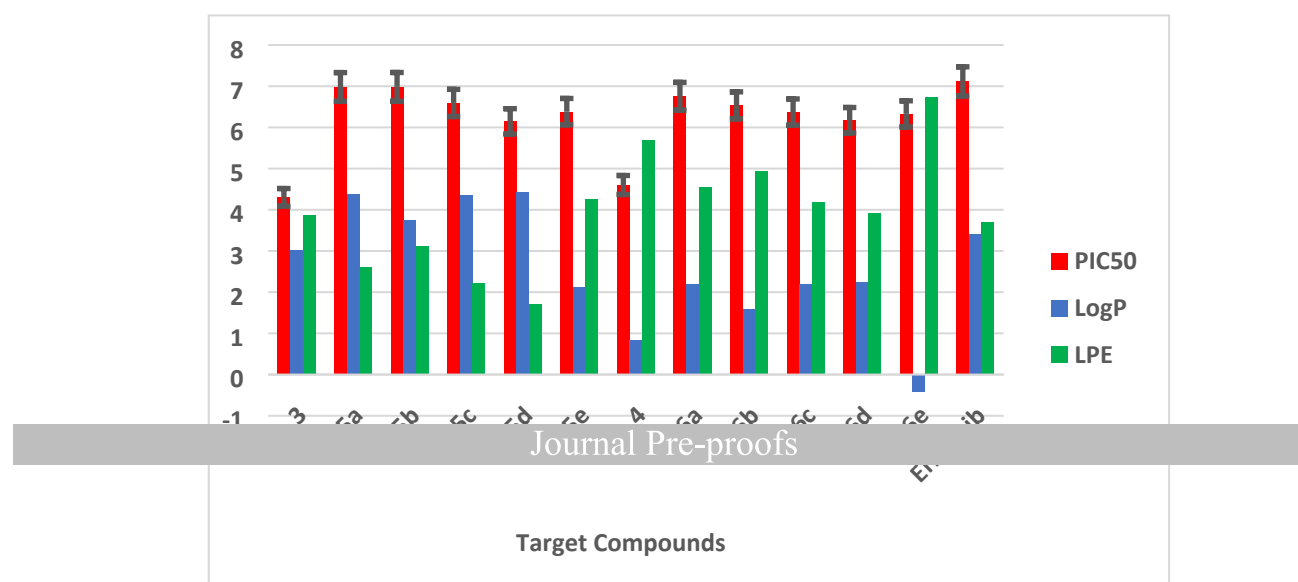


**Fig. 4.** Bar chart shows the distribution analysis of inhibitory activity ( $PIC_{50}$ ) of target compounds compared to LogP and LPE values. SE data were presented on red bars of activity.

### 2.3.1. Cell proliferation inhibitory activity

In-vitro anti-cancer activities of the compounds of interest were evaluated against three different cancer cell lines- MCF7 (Michigan cancer foundation-7, a breast cancer cell line), HCT116 (a human colorectal carcinoma cell lines) and HepG2 (a human liver carcinoma cell lines) following 3,(4,5-dimethylthiazole-2-yl)-2,5-diphenyltetrazolium bromide) tetrazolium (MTT) assay method [43, 44]. Staurosporine was employed as positive protein kinase inhibitor. The half maximal inhibitory ( $IC_{50}$ ) of the compounds of interest and that of positive control are presented in **Table 2** and in **Figure 1**.  $IC_{50}$  results indicate variable response to different cell lines.

**Table 2.** *In Vitro* Cell Growth Inhibitory Effects of compounds benzothiazole/isation-1,2,3-triazole-sulfa drug hybrids derivatives, and staurosporine against MCF-7, HCT116 and HepG2 cancer cell lines.

Cpd.	$IC_{50}$ ( $\mu M$ ) <sup>a</sup>		
	MCF-7	HCT-116	HepG2
<b>3</b>	3166±0.24	556±0.77	1002±0.1
<b>4</b>	4482±0.42	1797±1.4	646.2±0.33
<b>5a</b>	2.45±0.04	39±0.59	1.491±0.01
<b>5b</b>	23.8±0.38	58.6±1.3	1.786±0.01
<b>5c</b>	36.4±0.81	30.7±0.55	24.25±0.75
<b>5d</b>	6.01±0.07	36.4±0.95	6.305±0.04
<b>5e</b>	34.3±0.46	7.52±0.07	17.57±0.21
<b>6a</b>	36.6±0.93	37.4±0.74	2.594±0.07
<b>6b</b>	34.4±0.72	21.6±0.28	40.71±0.76
<b>6c</b>	12.3±0.12	46.2±0.93	9.817±0.10
<b>6d</b>	65.3±1.51	8.8±0.1	13.1±0.25
<b>6e</b>	33.5±0.33	17.4±0.29	91.04±0.33
<b>Staurosporine</b>	25.8±0.88	6.75±0.07	16.98±0.25

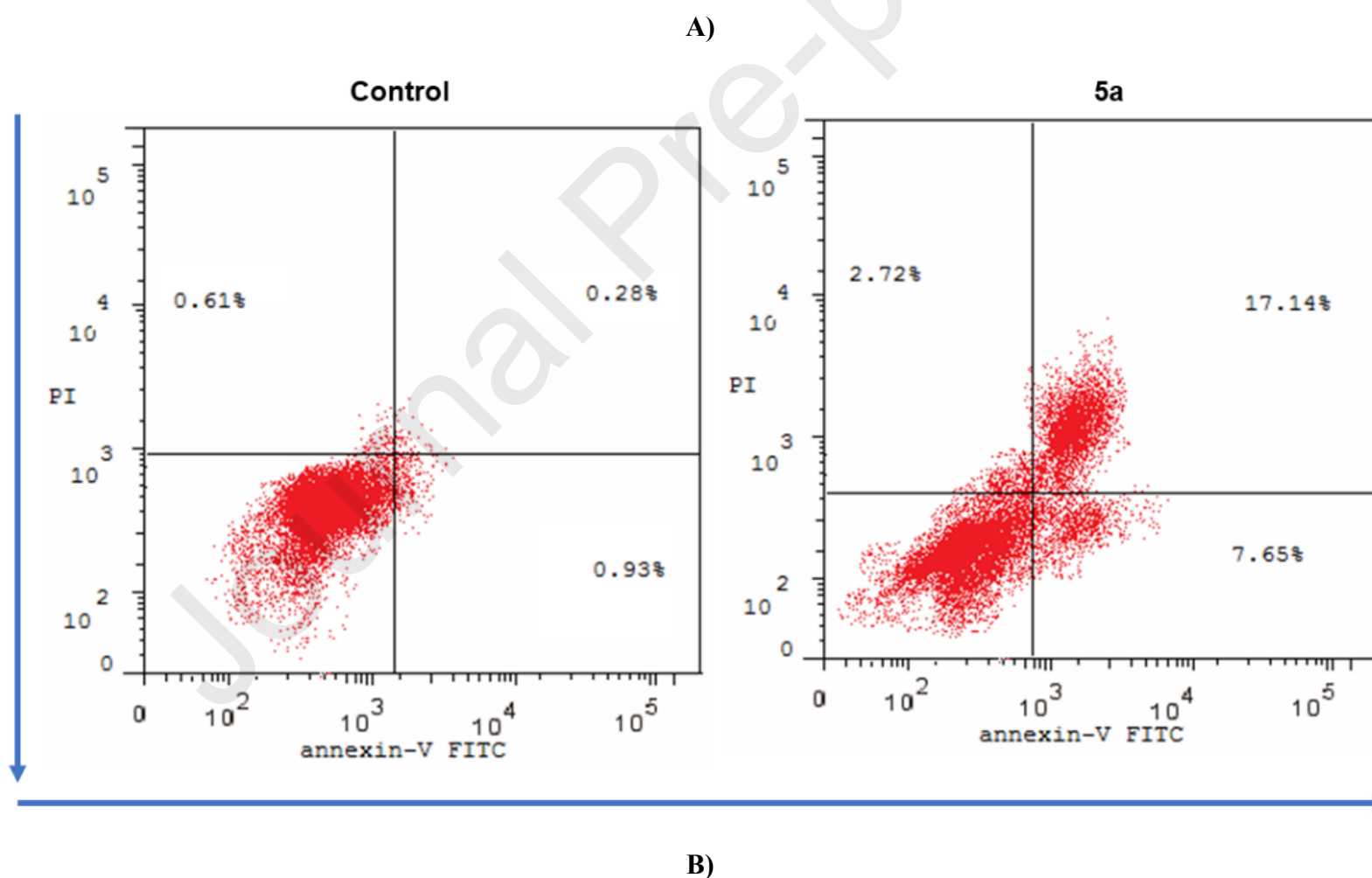
<sup>a</sup>  $IC_{50}$  values expressed in  $\mu M$  as the mean values of triplicate wells from at least three experiments and are reported as the mean  $\pm$  standard error. P-value is  $< 0.05$ .

Some of the newly designed click products displayed excellent to moderate growth inhibitory activity against the tested cancer cell lines. Compounds **5a** and **5b** were the most potent derivatives against cancer cell lines such as HepG2 with  $IC_{50}$  1.49±0.01 and 1.78±0.01  $\mu M$ , respectively, as compared to the standard Staurosporine with 16.98±0.25  $\mu M$ . While compounds **5a**, **5d**, **6c** and **3** arranged in the order of potency exhibited inhibitory activities on MCF7 cells with  $IC_{50}$  2.45±0.04, 6.01±0.07, 12.3±0.12 and 3166±0.24  $\mu M$ , respectively, compared to Staurosporine 25.8±0.88  $\mu M$ . Compounds **5e** and **6d** exhibited inhibition against HCT116 cells  $IC_{50}$  7.52±0.07 and 8.8±0.1 comparable to Staurosporine  $IC_{50}$  6.75±0.07  $\mu M$ . In particular, **5c**, **6b**, **6e** were inactive against these three control cell lines. Additionally, compounds **6a**, **6c**, **6d** and **5d** with  $IC_{50}$  2.59±0.07, 9.81±0.10, 13.1±0.25 and 6.30±0.04

$\mu\text{M}$ , respectively, possessed excellent antiproliferative activities against cancer cell line HepG2, compare to Staurosporine with  $\text{IC}_{50}$   $16.98 \pm 0.25$ . Also, **5b** and **6a** showed selectivity pattern against cancer cell lines HepG2. As a precaution test for normotoxic effect, **5a** the most active compound does not show any cytotoxicity against WI38 cells ( $520 \mu\text{M}$ ).

### 2.3.3. Cell apoptosis

Apoptosis induction was studied in HepG2 cells for three selected compounds based on the results from the EGFR assay results, **Table 1** and  $\text{IC}_{50}$  of compounds on different cell line, **Table 2**. Representative potent compounds **5a**, **5b** and **6a** were tested for apoptosis and their results were compared with untreated HepG2 cells which served as control for the experiment. Determined apoptosis with Annexin/PI double staining flow cytometric assay was presented in **Fig. 5A-C**. The percentage of total apoptotic cells (early and late apoptotic cells) increased from 2.72% for the control to 25 % in the case of compound **5a**, **Fig. 5A-B**. While the percentage of total apoptotic cells (early and late apoptotic cells) increased from 2.13% for the control to 30% in the case of compounds **5b** and **6a** induced apoptosis at a higher rate in HepG2 cells. Necrosis cell death leads to the release of the intracellular contents that affects neighboring cells and triggers an inflammatory reaction.[45] However, we did not observe cells undergoing necrosis upon treatment with compound **5a**, **5b** and **6a** (**Fig. 5B-C**) indicating that cells death occurred primarily through apoptosis. In cancer therapy, the most efficient and safe anticancer agent typically interfere with the balance between cell proliferation and apoptosis and shift cells toward the induction of apoptosis.[46] These results are consistent with other studies showing that erlotinib drug inhibits HepG2 tumor proliferation by inducing apoptosis, [47-49] as clearly detected for compounds.



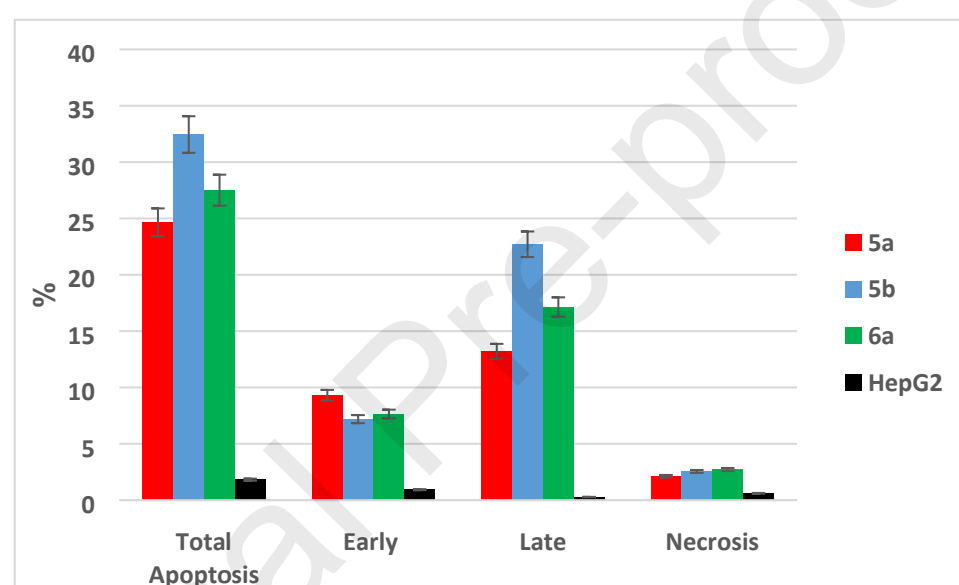
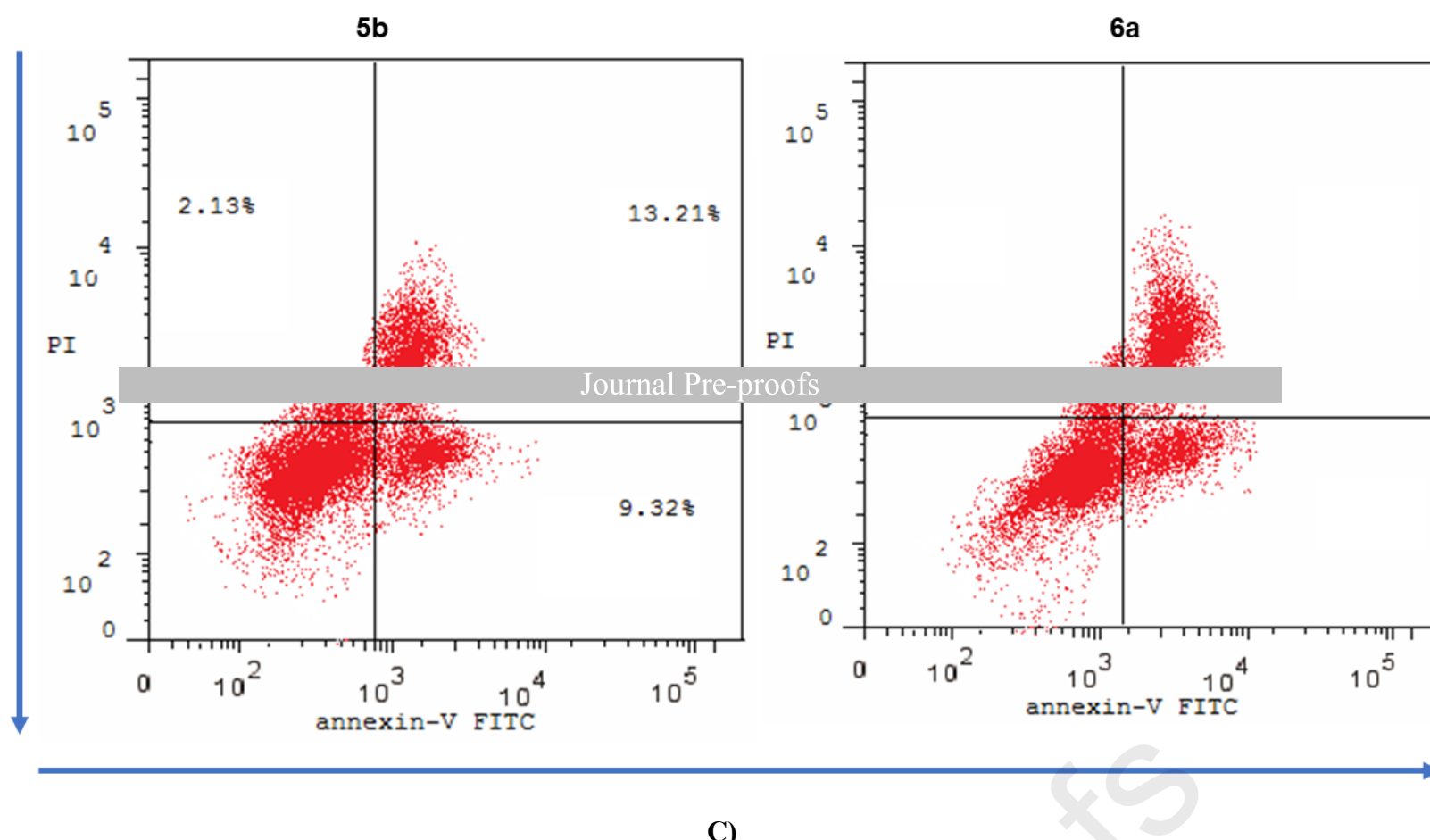
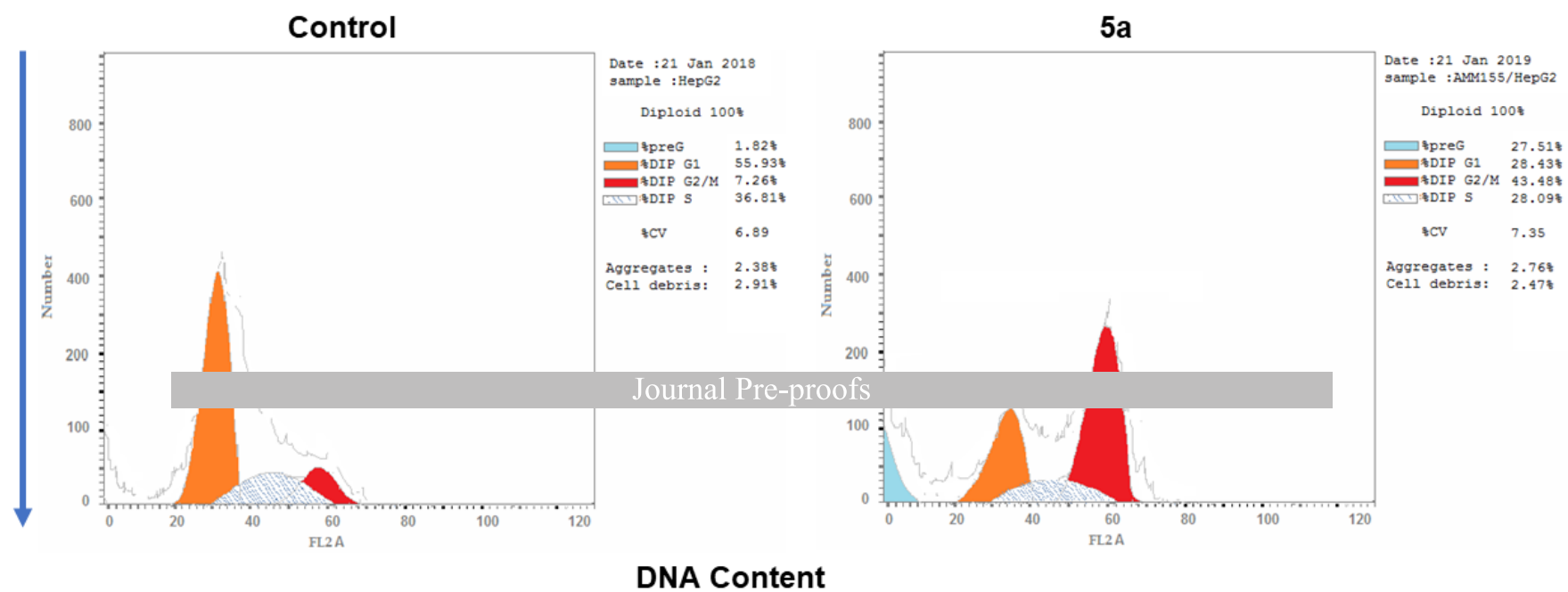


**Fig.5. A) and B)** Dot plot of Annexin V/PI double staining of HepG2 control and treated with analogues; **5a**, **5b**, and **6a**. **C)** Statistical analysis of the apoptosis percentage of **HepG2** cells after incubation with compounds **5a**, **5b**, and **6a** in conc. (1.87, 1.41, 0.7 $\mu$ g/mL respectively) for 24 h. The data are reported as the mean  $\pm$  SD of three independent experiments in triplicate.

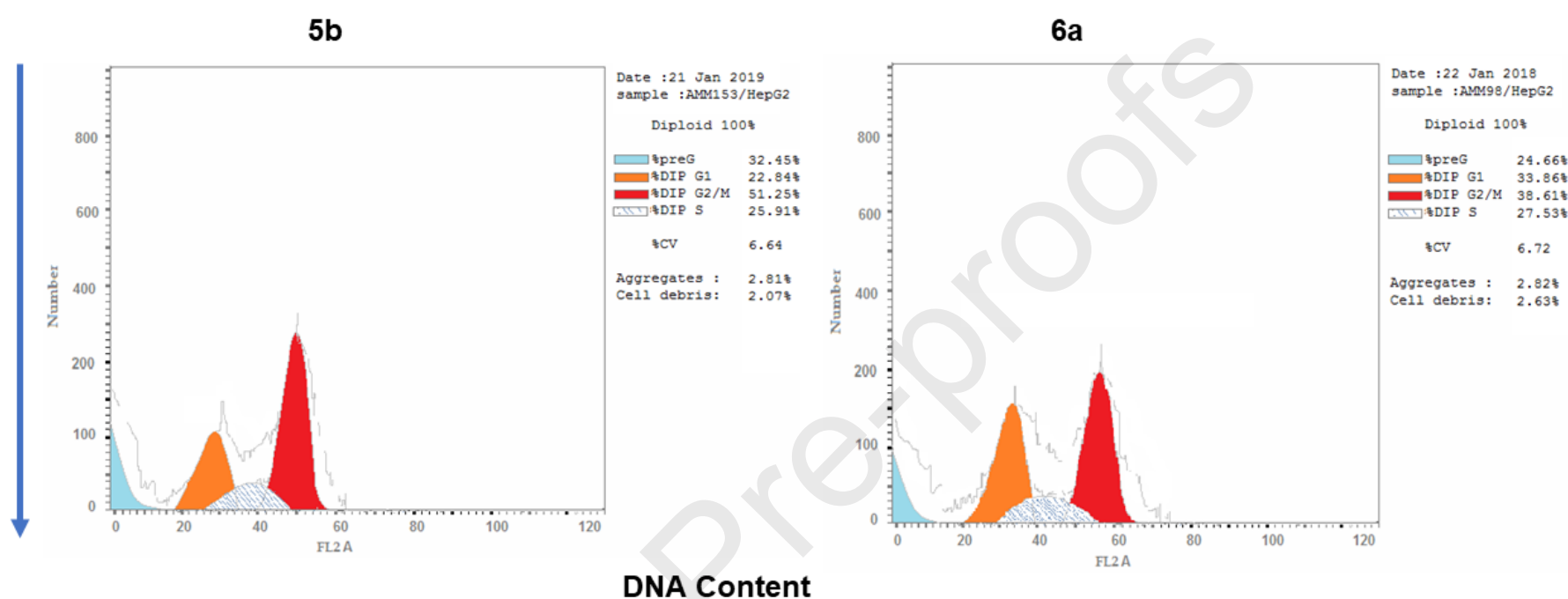
### 2.3.4. Cell cycle analysis

For the reduction of possible nonspecific effects of drugs in cancer treatment, the design and synthesis of novel chemotherapeutic agents that can regulate cell cycle progression and apoptosis is an attractive approach.[50] Therefore, further investigation of the effects of compound **5a**, **5b**, and **6a** on regulating cell cycle progression was explored using the Propidium Iodide Flow Cytometry Kit assay (**Fig. 6A-C**). The cell cycle histograms of the target HepG cancer cell treated with potent selected compounds (at IC<sub>50</sub> cytotoxicity) and compared to that of the untreated cells are illustrated in **Fig. 4**. The percentages of compound **5a** treated HepG cells in the G2/M phase were significantly higher than those in the control group. The distribution of cells in G1 and S phases was notably decreased compared to the control cells (**Fig. 6A**). The percentages of compound **5b** and **6a** treated HepG cells in the G2/M phase were significantly higher than those in the control group. The distribution of cells in G1 and S phases was notably decreased compared to the control cells (**Fig. 6B-C**). Previous studies showed that triazole-based EGFR drugs aligned along the microtubular network within the cells during the mitotic phase [51]. In addition, intracellular EGFR inhibitors have been associated with antimetabolic action.[52, 53] This might provide a possible explanation of cell cycle arrest observed at G2/M phase in cells treated with compounds **5a, 5b** and **6a**.

**A)**



B)



C)

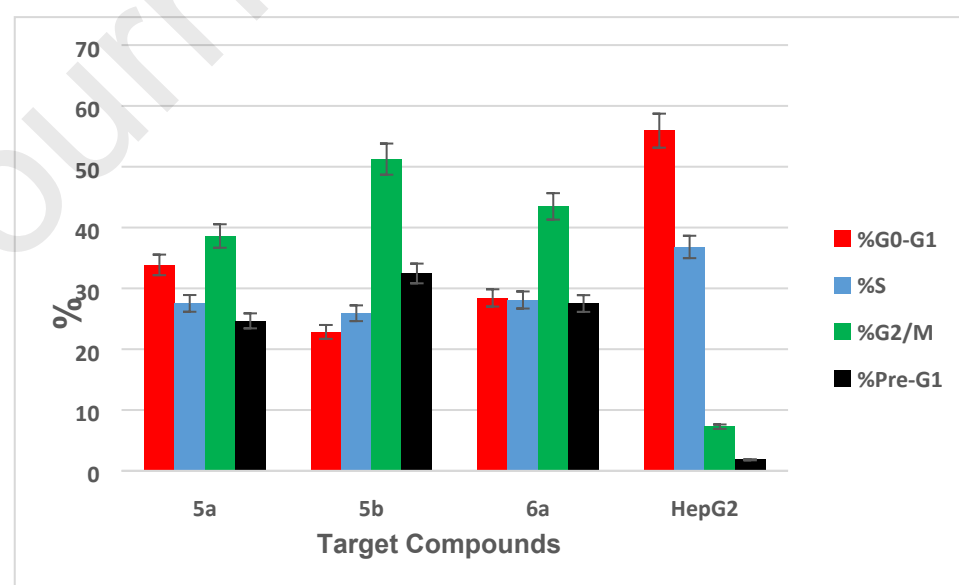


**Fig. 6.** A) and B) DNA content distribution histograms of control and treated cells. C) Statistical analysis of cell cycle phases percentage of **HepG2** cells after incubation with compounds **5a**, **5b**, **6a** (1.87, 1.41, 0.7 $\mu$ g/mL) for 24 h. The data are reported as the mean  $\pm$  SD of three independent experiments in triplicate. P-value is <0.05.

#### 2.4. EGFR target docking simulations

The integration process of experimental and computational methods is an extremely attractive strategy for the design and optimization of drug candidates [7, 54, 55]. Based upon the information obtained from the biology, molecular docking studies were performed as a crucial step toward understanding the mode of interaction of these novel compounds. The experiments were done on the basis of docking calculations using MOE [40] and Autodock.[56] From the Protein Data Bank [57] the X-ray structures of EGFR TK in complex with the erlotinib inhibitor (PDB entry 1M17) and used as template for docking. Compounds : Journal Pre-proofs .RMM force field and was then prepared for docking calculations with Python scripts available in the Autodock package. Prior to docking, bound crystallographic inhibitors were removed from the templates. For re-docking of crystallographic inhibitors as validation step and docking of compounds **5a** and **5b**, 50 flexible docking runs were performed using Autodock, and the resulting poses were clustered with 1.8 Å tolerance. Lamarckian genetic algorithm was used for the conformational space search with the initial population set to 150. The most populated clusters of low energy conformations were selected for analysis. For EGFR target, the applied docking protocol closely reproduced the experimental binding modes of re-docked inhibitors. Furthermore, the predicted binding modes of compounds **5a** and **5b** corresponded to the proposed fit of **5a** to the bound orientation of the crystallographic inhibitors. Previous studies [39, 58] have indicated that 4-anilinoquinazolines such as erlotinib cause inhibition through binding to the ATP site. The inhibitor was located well in the ATP pocket and anchored by Met769 through a hydrogen bond of 3.4 Å length to N quinazoline part, and affording more stability by hydrophobic interactions with Leu694, Leu820, Lys721, and Thr766 (hinge region; **Fig. 7A and D**) with binding energy = -21.5 Kcal/mol. We find our active compounds **5a** (binding energy = -20.5 Kcal/mol) and **5b** (binding energy = -19.75 Kcal/mol) bind as the same manner to reference erlotinib drug and showed strong H bonding with conserved Met769 residue (3.4 , 3.5 Å lengths for **5a** and **5b** respectively) through the conserved novel triazole N3 with consistent double aromatic stabilization with Leu694 and Gly772 residues in hinge region, **Fig. 7B-C**. This proves that the importance of triazole fragment as isostere for quinazoline ring. In addition, the terminal benzothiazole part exhibited quite similar interaction with Leu820 as hydrophobic conserved residue as did aniline aromatic part. The Asp831 acidic residues contributed for stabilization of benzothiazole in hydrophobic pocket more than aniline fragment. All behaviors of novel derivatives **5a** and **5b** in binding pocket were mapped to reference erlotinib drug as aligned structures in **Fig.7 D-E**. Encouragingly, the results of binding mode predictions for **5a** and **5b** were fully consistent with our 2D fitting as the underlying structure-based inhibitor design strategy. The novel scaffold was introduced for the first time as EGFR inhibitor and mapped with reference drugs could used as lead compound for design of low resistance anticancer agents.

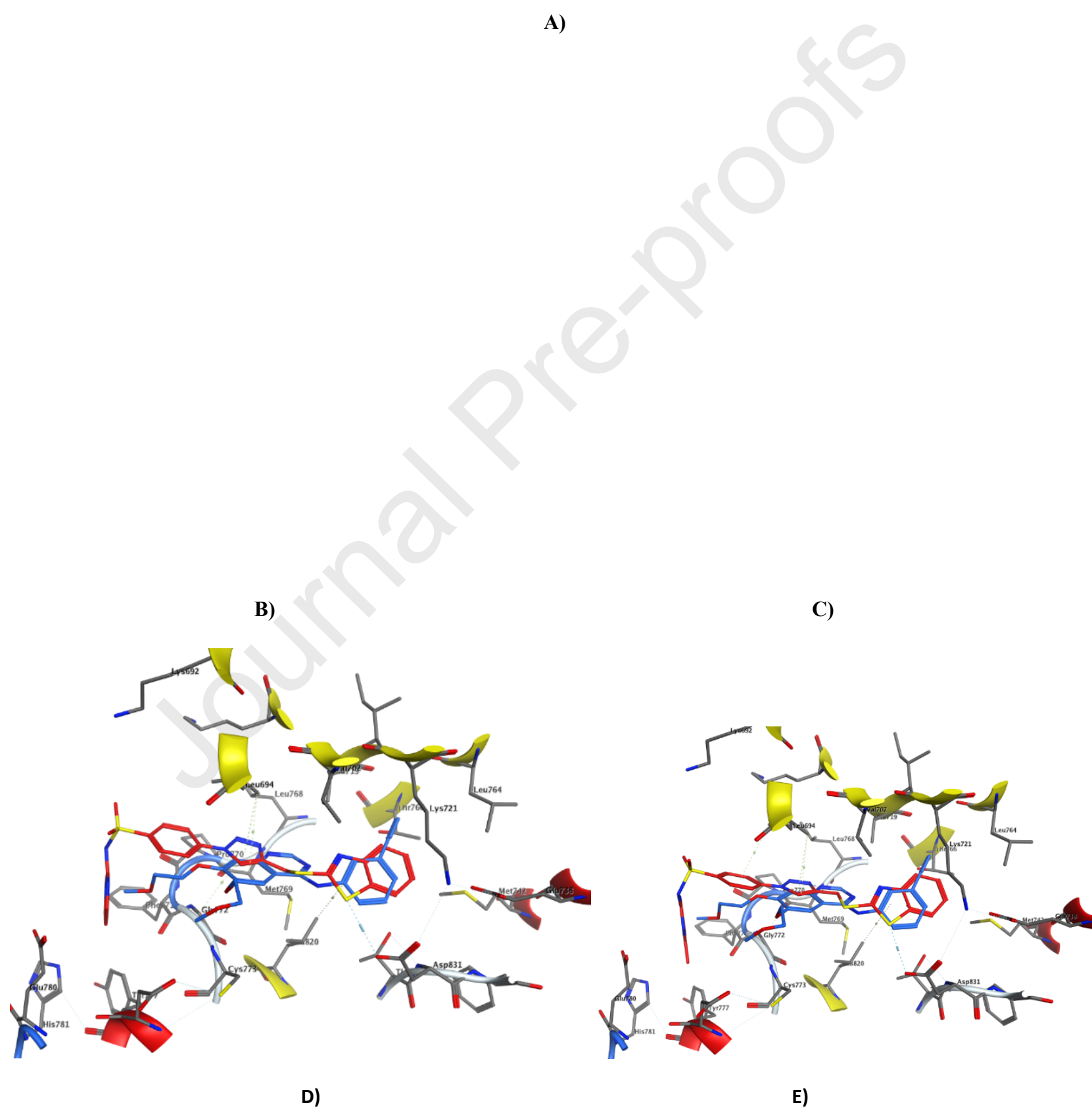


**Fig. 7.** Docking modes of active compound **5a** and **5b**. Shown are predicted complexes of **A) Erlotinib** drug with EGFR pocket; **B) Compound 5a** with EGFR ATP pocket; **C) Compound 5b** with EGFR ATP pocket; **D) Aligned 5a** with erlotinib in pocket; **E) Aligned 5b** with erlotinib in pocket. For comparison, the bound crystallographic inhibitors are shown. Carbon atoms of **5a** and **5b** and crystallographic reference inhibitors are colored red and blue, respectively. Possible hydrogen bonding interactions between compounds and EGFR are indicated by dashed lines.

### 3.2.5. Computational analysis of drug-likeness and ADME properties

PK properties such as absorption, distribution, metabolism, excretion and toxicity (ADMET) profiling of compounds were determined using the pkCSM ADMET descriptors algorithm protocol [59-61]. Two important chemical descriptors correlate well with PK properties, the 2D polar surface area (PSA\_2D, a primary determinant of fractional absorption) and the lipophilicity levels in the form of atom-based LogP. The absorption of drugs depends on factors including membrane permeability [indicated by colon cancer cell line (Caco-2)], intestinal absorption, skin permeability levels, P-glycoprotein substrate or inhibitor. The distribution of drugs depends on factors that include the blood–brain barrier (logBB), CNS permeability, and the volume of distribution (VDss). Metabolism is predicted based on the CYP models for substrate or inhibition (CYP2D6, CYP3A4, CYP1A2, CYP2C19, CYP2C9, CYP2D6, and CYP3A4). Excretion is predicted based on the total clearance model and renal OCT2 substrate. The toxicity of drugs is predicted based on AMES toxicity, hERG inhibition, hepatotoxicity, and skin sensitization. These parameters were calculated for potent **5a**, **5b** and less potent **6b** analogs compared to marketed drugs erlotinib and checked for compliance with their standard ranges. After calculating the ADMET properties (**Table 3**), we can verify that the ligands **5a**, **5b** and the reference erlotinib have almost similar Log P value (3.76, 4.37 and 3.40 respectively), while the ligand **6b** has low LogP value 1.58. On the other hand, we can verify that the ligands **5a**, **5b** and the reference erlotinib have a high percentage of human intestinal absorption (98.58%, 97.66% and 94.58% respectively), as they have very hydrophobic groups in their chemical structures, which would make it easy to pass through the biological membranes [61]. Conversely, **6b** has human intestinal absorption values less 90%, demonstrating that this compound may have poor oral bioavailability when tested experimentally [61]. Analyzing the central nervous system (CNS) permeability, **5a**, **5b** and erlotinib have good penetration in the CNS (-3.55 and -3.45 and -3.21 respectively), while **6b** is penetrate the CNS (Log PS <-3.50) [61]. These data may help that **5a** and **5b** present lower side effects in the (CNS) compare **6b**, contributing to a better tolerability among patients. It was also possible to observe that **5a**, **5b** and **6b** are able to inhibit the cytochrome P450, CYP3A4 isoform, the main enzyme responsible for drug metabolism. This possibly occurs because these ligands exhibit high molecular size, thus favoring the inhibition of this enzyme and may lead to interactions with other drugs metabolized by this CYP and may cause serious adverse effects [61]. The excretion was evaluated as Total Clearance. This parameter is related to bioavailability and is important in determining dosage rates to achieve steady state concentrations. Thus, these compounds, due to their high hydrophobicity, could not be excreted rapidly by the kidneys, requiring longer administration intervals to maintain desired therapeutic concentrations. The last parameter analyzed in our studies was hepatotoxicity. In (**Table 3**), we can verify that ligand showed hepatotoxic. Therefore, these ligands exhibit interaction with TcTR may not have a physiological or pathological event that could be associated with hepatic injury, suggesting that these compounds may be well tolerated by the liver when they are tested in a biological environment.

**Table 3.** Predicted ADMET properties of selective target compounds.

Parameter	5b	5a	6b	Erlotinib
<b>Molecular properties</b>				
Molecular Weight	481.58	509.64	461.46	393.44
LogP	3.76	4.37	1.58	3.40
Rotatable Bonds	7	7	6	10
Acceptors	10	10	9	7
Donors	1	1	1	1
Surface Area	191.17	203.90	187.32	169.53
<b>Absorption</b>				
Water solubility	-3.09	-3.28	-3.45	-4.73
Caco2 permeability	0.56	0.60	0.19	1.43
Intestinal absorption (human)	97.66	98.58	86.67	94.58
Skin Permeability	-2.73	-2.73	-2.73	-2.74
P-glycoprotein substrate	Yes	Yes	No	No
P-glycoprotein I inhibitor	Yes	Yes	Yes	Yes
P-glycoprotein II inhibitor	Yes	Yes	Yes	Yes
<b>Distribution</b>				
VDss (human)	0.114	0.136	-0.40	0.199
Fraction unbound (human)	0.091	0.084	0.144	0.059
BBB permeability	-1.818	-1.807	-1.807	-0.745
CNS permeability	-3.55	-3.45	-3.97	-3.21
<b>Metabolism</b>				
CYP2D6 substrate	No	No	No	No

CYP3A4 substrate	Yes	Yes	Yes	Yes
CYP1A2 inhibitor	No	No	Yes	Yes
CYP2C19 inhibitor	Yes	No	No	Yes
CYP2C9 inhibitor	Yes	Yes	No	Yes
CYP2D6 inhibitor	No	No	No	No
CYP3A4 inhibitor	Yes	Yes	Yes	Yes
<b>Excretion</b>				
Total Clearance	0.178	0.066	0.165	0.702
Renal OCT2 substrate	Yes	No	No	No
<b>Toxicity</b>				
Journal Pre-proofs				
Max. tolerated dose (human)	0.573	0.545	0.672	0.839
hERG I inhibitor	No	No	No	No
hERG II inhibitor	Yes	Yes	Yes	Yes
Oral Rat Acute Toxicity (LD <sub>50</sub> )	2.69	2.79	2.81	2.39
Oral Rat Chronic Toxicity (LOAEL)	0.31	0.31	0.47	1.37
Hepatotoxicity	Yes	Yes	Yes	Yes
Skin Sensitization	No	No	No	No
T. Pyriformis toxicity	0.285	0.285	0.285	0.309
Minnow toxicity	-1.739	-1.503	-1.105	-0.102

### 3.2.6. SAR analysis of target compounds

The above analyses suggested different preliminary SARs for the triazole anticancer agent scaffold that mimics the quinazoline-based inhibitors targeting EGFR TK, that can be summarized in **Fig. 8**. Different factors affect activity; the terminal aromatic part whether benzothiazole or isatin, linker to aromatic part, and terminal sulpha fragments. The installation of benzothiazole affording more active anticancer and EGFR inhibitors than isatin moiety that behaves as more aromatic system and able to accommodate by aromatic hydrophobic interactions. In addition, the S linker to triazole scaffold combined with benzothiazole part increases the activity than no linker in case of isatin. As well, the sulpha parts used in synthesis of final analogs also showed prominent increase in activity according to their structures of terminal part. Full 6-membered aromatic systems with small methyl substituents are of great importance in anticancer and EGFR activity and are favorable for interactions.

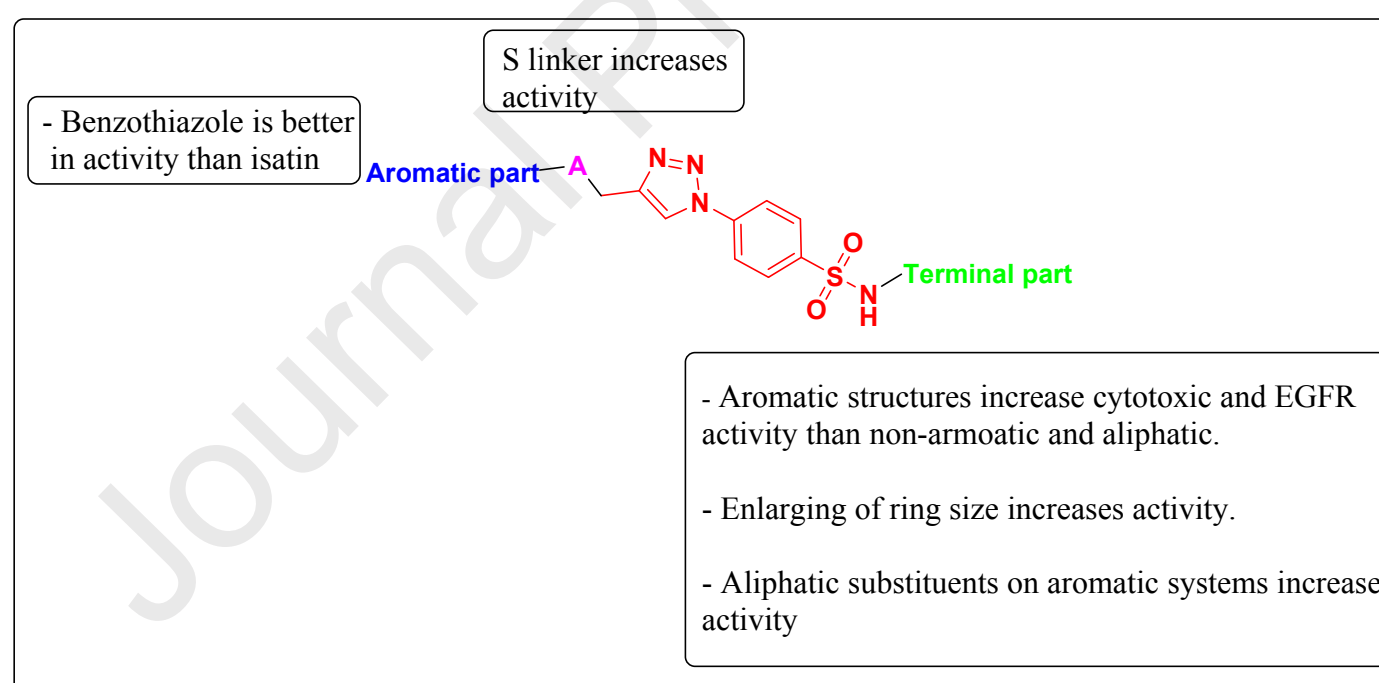


**Fig. 8.** Summary of the SARs of triazole-based EGFR anticancer derivatives.

## 4. Concluding remarks

In this study, a series of cytotoxic agents 1,2,3 triazole-based compounds containing different aromatic substructures and different sulpha termini have been designed, synthesized, mimics quinazoline-based EGFR inhibitors and thus evaluated for EGFR inhibitory activity. Most of the synthesized derivatives had promising activity compared to reference inhibitor. Compounds of benzothiazole offered more potency than isatin ones and especially **5a** and **5b** were the most potent EGFR inhibitors with IC<sub>50</sub> values of 103 nM and 104 nM, respectively. We also evaluated anti-proliferative activities of the novel compounds against MCF-7, HCT-116, and HepG2 cells and found them with remarkable promising activity compared to the reference drug. However, the pyridine and methylpyridine derivatives of benzothiazole series **5a** and **5b** were the most effective cytotoxic agents. In addition, upon treatment of HepG2 cells with the most active derivatives **5a** and **5b**, they cause cell cycle arrest observed at G2/M phase. Finally, we discovered

a novel triazole-based analogue with remarkable cytotoxicity and EGFR inhibitory activity that might be further subjected for extensive optimization to offer a new anticancer compounds.

### 3. Experimental Section

#### 3.1. General Information

All reagents and solvents used were of the highest quality of analytical reagent grade and were used without further purification. Fine chemicals including 2-mercaptobenzothiazole, Isatin and potassium carbonate were purchased from BDH Chemicals Ltd, UK. The other fine chemicals used were sulfamethazine, sulfadiazine, sulfapyridine, sulfathiazole and sulfaguanidine sodium azide, sodium nitrate, triethylamine, propargyl bromide (80 wt % in toluene), CuSO<sub>4</sub> and Na-ascorbate (Sigma-Aldrich, USA). The solvents used ethyl acetate, hexane, ethanol and DMF were purchased from Sigma-Aldrich, USA. Melting points were measured on a Stuart Scientific SMP1 and are uncorrected. TLC was performed on UV fluorescent Silical gel Merck 60 F254 plates, and the spots were visualized using a UV lamp (254 nm). SHIMADZU FTIR-8400S spectrometer was used for identification of functional groups in the range of 4000-400 cm<sup>-1</sup>. The NMR spectra were run with Bruker spectrometer (400 MHz) with TMS as internal reference.

#### **Synthesis and characterization of 2-(prop-2-yn-1-ylthio)benzo[d]thiazole (3)**

To a mixture of 2-mercaptobenzothiazole (10 mmol), triethylamine (11 mmol) and ethanol (20 ml) was added with stirring propargyl bromide (15 mmol). The mixture was stirred at reflux for 2 h. Ethanol was removed under pressure and the resulting solid was collected and recrystallized from ethanol to afford the targeted alkyne **3** as white pellets, 91 %, mp: 80-81 °C (lit. mp: 82-83 °C [[34]]). IR ( $\nu$ , cm<sup>-1</sup>): 1590 (C=C), 1610 (C=N), 2150 (C≡C), 2940 (C-H al), 3060 (C-H ar), 3310 (≡CH). <sup>1</sup>H NMR (400 MHz, CDCl<sub>3</sub>):  $\delta_{\text{H}}$  2.33 (s, 1H, ≡CH), 4.16 (s, 2H, SCH<sub>2</sub>), 7.33 (t, 1H, *J* = 8.0 Hz, Ar-H), 7.45 (t, 1H, *J* = 8.0 Hz, Ph-H), 7.79 (d, 1H, *J* = 8.0 Hz, Ph-H), 7.94 (d, 1H, *J* = 8.0 Hz, Ar-H). <sup>13</sup>C NMR (100 MHz, CDCl<sub>3</sub>):  $\delta_{\text{C}}$  21.62 (SCH<sub>2</sub>); 72.39, 78.35 (C≡C); 121.11, 121.85, 124.54, 126.28, 135.49, 153.03, 164.60 (Ar-C, C=N) ppm.

#### **Synthesis and characterization of 1-(prop-2-yn-1-yl)indoline-2,3-dione (4)**

A mixture of isatin (10 mmol), potassium carbonate (11 mmol) in DMF (25 mL) was stirred at room temperature for 2 h. Then, propargyl bromide (15 mmol) was added and the reaction mixture was stirred at room temperature overnight. The mixture was poured onto crushed ice water and the precipitate thus formed was collected by filtration and recrystallized from ethanol to afford the desired alkyne **4** as orange crystals, 95 %, mp: 155-156 °C (lit. mp: 157-158 [[34]]). IR ( $\nu$ , cm<sup>-1</sup>): 1570 (C=C), 1610 (C=N), 1720 (C=O), 2150 (C≡C), 2930 (C-H al), 3050 (C-H ar), 3310 (≡CH). <sup>1</sup>H NMR (400 MHz, CDCl<sub>3</sub>):  $\delta$  = 2.33 (s, 1H, ≡CH), 4.55 (s, 2H, NCH<sub>2</sub>), 7.14-7.21 (m, 2H, Ar-H), 7.64-7.68 (m, 2H, Ar-H). <sup>13</sup>C NMR (100 MHz, CDCl<sub>3</sub>):  $\delta$  = 29.46 (SCH<sub>2</sub>); 73.37, 75.68 (C≡C); 111.11, 117.68, 124.23, 125.49, 138.46, 149.61, 151.22, 182.56 (Ar-C, C=N, C=O) ppm.

#### **General procedure for the synthesis of 1,4-disubstituted-1,2,3-triazoles 5a-e and 6a-e**

A solution of copper sulfate (0.10 g) and sodium ascorbate (0.15 g) in water (10 mL) was added with stirring to a solution of the appropriate heterocyclic alkyne **3** and/or **4** (1 mmol) in DMSO (10 mL). Thereafter, the appropriate sulfa-drug azide **2a-e** (1 mmol) was added, and the reaction mixture was stirred at room temperature for 8-12 h, until the consumption of the starting material as indicated by TLC (hexane-ethyl acetate). The iced-water was added in the mixture and the precipitate thus formed was collected by filtration, washed with saturated solution of ammonium chloride and recrystallized from ethanol/DMF to give the targeted 1,2,3-triazoles **5a-e** and **6a-e**.

#### **Characterization of the click products 5a-e and 6a-e**

##### **4-(4-((Benzo[d]thiazol-2-ylthio)methyl)-1H-1,2,3-triazol-1-yl)-N-(4,6-dimethylpyrimidin-2-yl)benzenesulfonamide (5a)**

Green solid; Yield: 85 %; mp: 195-196 °C; IR ( $\nu$ , cm<sup>-1</sup>): 1560 (C=C), 1610 (C=N), 2960 (C-H al), 3060 (C-H Ar), 3370 (N-H). <sup>1</sup>H NMR (400 MHz, DMSO-*d*<sub>6</sub>)  $\delta_{\text{H}}$  = 2.24 (s, 6H, 2 x CH<sub>3</sub>), 4.79 (s, 2H, SCH<sub>2</sub>), 6.67 (bs, 1H, Ar-H), 7.37 (t, 1H, *J* = 8.0 Hz, Ar-H), 7.47 (t, 1H, *J* = 8.0 Hz, Ar-H), 7.93 (d, 1H, *J* = 8.0 Hz, Ar-H), 8.00-8.11 (m, 5H, Ar-H), 8.91 (s, 1H, CH-1,2,3-triazole), 12.56 (bs, 1H, NH). <sup>13</sup>C NMR (100 MHz, DMSO-*d*<sub>6</sub>)  $\delta_{\text{C}}$  = 27.68 (SCH<sub>2</sub>); 29.48 (CH<sub>3</sub>); 121.77, 122.33, 122.79, 125.06, 126.88, 130.22, 135.19, 144.90, 153.02, 166.03 (Ar-C, C=N); Found: C, 47.66; H, 3.27; N, 17.59; C<sub>16</sub>H<sub>13</sub>N<sub>5</sub>O<sub>2</sub>S<sub>3</sub> requires C, 47.63; H, 3.25; N, 17.36.

##### **4-(4-((Benzo[d]thiazol-2-ylthio)methyl)-1H-1,2,3-triazol-1-yl)-N-(pyrimidin-2-yl)benzenesulfonamide (5b)**

Green solid; Yield: 86 %; mp: 204-205 °C; IR ( $\nu$ , cm<sup>-1</sup>): 1575 (C=C), 1615 (C=N), 2945 (C-H al), 3045 (C-H Ar), 3370 (N-H). <sup>1</sup>H NMR (400 MHz, DMSO-*d*<sub>6</sub>)  $\delta_{\text{H}}$  = 4.80 (s, 2H, SCH<sub>2</sub>), 7.30-7.35 (m, 3H, Ar-H), 7.41-7.46 (m, 2H, Ar-H), 7.91-7.98 (m, 5H, Ar-H), 8.29 (bs, 1H, Ar-H), 8.93 (s, 1H, CH-1,2,3-triazole), 12.58 (bs, 1H, NH). <sup>13</sup>C NMR (100 MHz, DMSO-*d*<sub>6</sub>)  $\delta_{\text{C}}$  = 27.72 (SCH<sub>2</sub>); 121.77, 122.32, 125.03, 126.87, 135.21, 153.02, 166.05 (Ar-C, C=N); Found: C, 49.80; H, 3.16; N, 20.54; C<sub>20</sub>H<sub>15</sub>N<sub>7</sub>O<sub>2</sub>S<sub>3</sub> requires C, 49.88; H, 3.14; N, 20.36.

##### **4-(4-((Benzo[d]thiazol-2-ylthio)methyl)-1H-1,2,3-triazol-1-yl)-N-(pyridin-2-yl)benzenesulfonamide (5c)**

Green solid; Yield: 85 %; mp: 231-232 °C; IR ( $\nu$ ,  $\text{cm}^{-1}$ ): 1570 (C=C), 1615 (C=N), 2960 (C-H al), 3070 (C-H Ar), 3335 (N-H).  $^1\text{H}$  NMR (400 MHz,  $\text{DMSO-}d_6$ )  $\delta_{\text{H}} = 4.80$  (s, 2H,  $\text{SCH}_2$ ), 6.86 (bs, 1H, Ar-H), 7.22 (bs, 1H, Ar-H), 7.34-7.38 (m, 1H, Ar-H), 7.45-7.48 (m, 1H, Ar-H), 7.76 (bs, 1H, Ar-H), 7.91-8.05 (m, 7H, Ar-H), 8.92 (s, 1H, CH-1,2,3-triazole), 12.60 (bs, 1H, NH).  $^{13}\text{C}$  NMR (100 MHz,  $\text{DMSO-}d_6$ )  $\delta_{\text{C}} = 27.72$  ( $\text{SCH}_2$ ); 120.80, 121.78, 122.33, 122.83, 125.05, 126.87, 128.72, 135.20, 144.58, 153.02, 166.05 (Ar-C, C=N); Found: C, 52.45; H, 3.34; N, 17.35;  $\text{C}_{21}\text{H}_{16}\text{N}_6\text{O}_2\text{S}_3$  requires C, 52.48; H, 3.36; N, 17.49.

**4-(4-((Benzo[d]thiazol-2-ylthio)methyl)-1H-1,2,3-triazol-1-yl)-N-(thiazol-2-yl)benzenesulfonamide (5d)**

Green solid; Yield: 84 %; mp: 180-181 °C; IR ( $\nu$ ,  $\text{cm}^{-1}$ ): 1570 (C=C), 1625 (C=N), 2945 (C-H al), 3070 (C-H Ar), 3385 (N-H).  $^1\text{H}$  NMR (400 MHz,  $\text{DMSO-}d_6$ )  $\delta_{\text{H}} = 4.79$  (s, 2H,  $\text{SCH}_2$ ), 6.86 (bs, 1H, Ar-H), 7.22 (bs, 1H, Ar-H), 7.34-7.38 (m, 1H, Ar-H), 7.45-7.48 (m, 1H, Ar-H), 7.76 (bs, 1H, Ar-H), 7.91-8.05 (m, 7H, Ar-H), 8.92 (s, 1H, CH-1,2,3-triazole), 12.60 (bs, 1H, NH).  $^{13}\text{C}$  NMR (100 MHz,  $\text{DMSO-}d_6$ )  $\delta_{\text{C}} = 27.68$  ( $\text{SCH}_2$ ); 120.88, 121.78, 122.32, 125.04, 126.88, 127.95, 135.19, 138.87, 153.01, 166.01 (Ar-C, C=N); Found: C, 46.87; H, 3.01; N, 17.23;  $\text{C}_{19}\text{H}_{14}\text{N}_6\text{O}_2\text{S}_4$  requires C, 46.90; H, 2.90; N, 17.27.

**4-(4-((Benzo[d]thiazol-2-ylthio)methyl)-1H-1,2,3-triazol-1-yl)-N-(diaminomethylene)-benzenesulfonamide (5e)**

Green solid; Yield: 90 %; mp: 264-265 °C; IR ( $\nu$ ,  $\text{cm}^{-1}$ ): 1580 (C=C), 1610 (C=N), 2965 (C-H al), 3040 (C-H Ar), 3250-3370 ( $\text{NH}_2$ ).  $^1\text{H}$  NMR (400 MHz,  $\text{DMSO-}d_6$ )  $\delta_{\text{H}} = 4.81$  (s, 2H,  $\text{SCH}_2$ ), 6.79 (bs, 4H, 2 x  $\text{NH}_2$ ), 7.37 (t, 1H,  $J = 8.0$  Hz, Ar-H), 7.48 (t, 1H,  $J = 8.0$  Hz, Ar-H), 7.91-7.94 (m, 3H, Ar-H), 8.01-8.04 (m, 3H, Ar-H), 8.92 (s, 1H, CH-1,2,3-triazole).  $^{13}\text{C}$  NMR (150 MHz,  $\text{DMSO-}d_6$ )  $\delta_{\text{C}} = 27.70$  ( $\text{SCH}_2$ ), 120.66, 121.78, 122.34, 122.81, 125.06, 126.89, 127.84, 135.21, 138.49, 144.48, 144.79, 153.03, 158.63, 166.03 (Ar-C, C=N); Found: C, 45.81; H, 3.36; N, 21.97;  $\text{C}_{17}\text{H}_{15}\text{N}_7\text{O}_2\text{S}_3$  requires C, 45.83; H, 3.39; N, 22.01.

**N-(4,6-Dimethylpyrimidin-2-yl)-4-(4-((2,3-dioxindolin-1-yl)methyl)-1H-1,2,3-triazol-1-yl)benzenesulfonamide (6a)**

Orange crystals; Yield: 90 %; mp: 211-212 °C; IR ( $\nu$ ,  $\text{cm}^{-1}$ ): 1560 (C=C), 1610 (C=N), 1730 (C=O), 2950 (C-H al), 3070 (C-H Ar), 3340 (N-H).  $^1\text{H}$  NMR (400 MHz,  $\text{DMSO-}d_6$ )  $\delta_{\text{H}} = 2.26$  (s, 6H, 2 x  $\text{CH}_3$ ), 5.10 (s, 2H,  $\text{NCH}_2$ ), 6.70-6.74 (m, 1H, Ar-H), 7.10-7.19 (m, 2H, Ar-H), 7.61-7.66 (m, 2H, Ar-H), 7.97-8.14 (m, 4H, Ar-H), 8.96 (bs, 1H, CH-1,2,3-triazole), 12.31 (bs, 1H, NH).  $^{13}\text{C}$  NMR (100 MHz,  $\text{DMSO-}d_6$ )  $\delta_{\text{C}} = 27.75$  ( $\text{CH}_3$ ), 34.93 ( $\text{NCH}_2$ ), 110.98, 117.81, 119.45, 122.31, 124.65, 129.35, 132.34, 133.07, 138.24, 139.15, 140.45, 143.25, 149.86, 155.95, 158.05, 158.56 (Ar-C, C=N), 182.74 (C=O); Found: C, 56.40; H, 3.88; N, 20.01;  $\text{C}_{23}\text{H}_{19}\text{N}_7\text{O}_4\text{S}$  requires C, 56.43; H, 3.91; N, 20.03.

**4-(4-((2,3-Dioxindolin-1-yl)methyl)-1H-1,2,3-triazol-1-yl)-N-(pyrimidin-2-yl)benzenesulfonamide (6b)**

Orange crystals; Yield: 88 %; mp: 234-235 °C; IR ( $\nu$ ,  $\text{cm}^{-1}$ ): 1575 (C=C), 1620 (C=N), 1725 (C=O), 2970 (C-H al), 3045 (C-H Ar), 3370 (N-H).  $^1\text{H}$  NMR (400 MHz,  $\text{DMSO-}d_6$ )  $\delta_{\text{H}} = 5.08$  (s, 2H,  $\text{NCH}_2$ ), 7.03-7.07 (m, 1H, Ar-H), 7.12-7.20 (m, 2H, Ar-H), 7.58-7.65 (m, 2H, Ar-H), 8.05-8.08 (m, 2H, Ar-H), 8.13-8.17 (m, 2H, Ar-H), 8.51 (d, 2H,  $J = 4.0$  Hz, Ar-H), 8.95 (s, 1H, CH-1,2,3-triazole), 12.02 (bs, 1H, NH).  $^{13}\text{C}$  NMR (100 MHz,  $\text{DMSO-}d_6$ )  $\delta_{\text{C}} = 34.99$  ( $\text{NCH}_2$ ), 111.06, 117.68, 119.96, 122.07, 123.40, 124.45, 129.46, 129.58, 138.10, 139.08, 140.22, 143.18, 149.98, 156.64, 157.83, 158.33 (Ar-C, C=N), 182.96 (C=O); Found: C, 54.56; H, 3.25; N, 21.27;  $\text{C}_{21}\text{H}_{15}\text{N}_7\text{O}_4\text{S}$  requires C, 54.66; H, 3.28; N, 21.25.

**4-(4-((2,3-Dioxindolin-1-yl)methyl)-1H-1,2,3-triazol-1-yl)-N-(pyridin-2-yl)benzenesulfonamide (6c)**

Orange crystals; Yield: 89 %; mp: 248-249 °C; IR ( $\nu$ ,  $\text{cm}^{-1}$ ): 1565 (C=C), 1610 (C=N), 1730 (C=O), 2960 (C-H al), 3075 (C-H Ar), 3350  $\text{cm}^{-1}$  (N-H).  $^1\text{H}$  NMR (400 MHz,  $\text{DMSO-}d_6$ )  $\delta_{\text{H}} = 5.08$  (s, 2H,  $\text{NCH}_2$ ), 6.85 (s, 1H, Ar-H), 7.12-7.20 (m, 3H, Ar-H), 7.58-7.65 (m, 2H, Ar-H), 7.73-7.77 (m, 1H, Ar-H), 7.97-8.03 (m, 5H, Ar-H), 8.93 (s, 1H, CH-1,2,3-triazole), 12.45 (bs, 1H, NH).  $^{13}\text{C}$  NMR (100 MHz,  $\text{DMSO-}d_6$ )  $\delta_{\text{C}} = 34.99$  ( $\text{NCH}_2$ ), 110.08, 117.67, 120.12, 122.02, 123.40, 124.45, 128.25, 138.10, 138.48, 143.10, 150.00, 157.83 (Ar-C, C=N), 182.96 (C=O), Found: C, 57.56; H, 3.23; N, 18.23;  $\text{C}_{22}\text{H}_{16}\text{N}_6\text{O}_4\text{S}$  requires C, 57.38; H, 3.50; N, 18.25.

**4-(4-((2,3-Dioxindolin-1-yl)methyl)-1H-1,2,3-triazol-1-yl)-N-(thiazol-2-yl)benzenesulfonamide (6d)**

Orange crystals; Yield: 86 %; mp: 260-263 °C; IR ( $\nu$ ,  $\text{cm}^{-1}$ ): 1580 (C=C), 1615 (C=N), 1720 (C=O), 2940 (C-H al), 3055 (C-H Ar), 3380  $\text{cm}^{-1}$  (N-H).  $^1\text{H}$  NMR (400 MHz,  $\text{DMSO-}d_6$ )  $\delta_{\text{H}} = 5.08$  (s, 2H,  $\text{NCH}_2$ ), 6.86 (bs, 1H, Ar-H), 7.12-7.21 (m, 3H, Ar-H), 7.58-7.66 (m, 2H, Ar-H), 7.97-8.03 (m, 4H, Ar-H), 8.93 (s, 1H, CH-1,2,3-triazole), 12.83 (bs, 1H, NH).  $^{13}\text{C}$  NMR (100 MHz,  $\text{DMSO-}d_6$ )  $\delta_{\text{C}} = 34.99$  ( $\text{NCH}_2$ ), 111.07, 117.70, 120.18, 121.92, 123.40, 124.46, 127.60, 138.10, 138.61, 143.17, 150.03, 157.85 (Ar-C, C=N), 182.89 (C=O), Found: C, 51.50; H, 3.06; N, 17.94;  $\text{C}_{20}\text{H}_{14}\text{N}_6\text{O}_4\text{S}_2$  requires C, 51.49; H, 3.02; N, 18.02.

**N-(Diaminomethylene)-4-(4-((2,3-dioxindolin-1-yl)methyl)-1H-1,2,3-triazol-1-yl)benzenesulfonamide (6e)**

Orange crystals; Yield: 91 %; mp: 270-271 °C; IR ( $\nu$ ,  $\text{cm}^{-1}$ ): 1560 (C=C), 1625 (C=N), 1715 (C=O), 2930 (C-H al), 3065 (C-H Ar), 3330-3445  $\text{cm}^{-1}$  (N-H).  $^1\text{H}$  NMR (400 MHz,  $\text{DMSO-}d_6$ )  $\delta_{\text{H}} = 5.09$  (s, 2H,  $\text{NCH}_2$ ), 6.78 (bs, 4H, 2 x  $\text{NH}_2$ ), 7.15 (t, 1H,  $J = 8.0$  Hz, Ar-H), 7.22 (d, 1H,  $J = 8.0$  Hz, Ar-H), 7.61 (d, 1H,  $J = 8.0$  Hz, Ar-H), 7.65 (t, 1H,  $J = 8.0$  Hz, Ar-H), 7.92-8.01 (m, 4H, Ar-H), 8.95 (s, 1H, CH-1,2,3-triazole).  $^{13}\text{C}$  NMR (100 MHz,  $\text{DMSO-}d_6$ )  $\delta_{\text{C}} = 35.48$  ( $\text{NCH}_2$ ), 111.58, 118.19, 120.44, 122.48, 123.90, 124.98, 127.87, 138.47, 138.60, 143.60, 144.80, 150.49, 158.36, 158.63 (Ar-C, C=N), 183.49 (C=O), Found: C, 50.79; H, 3.49; N, 23.01;  $\text{C}_{18}\text{H}_{15}\text{N}_7\text{O}_4\text{S}$  requires C, 50.82; H, 3.55; N, 23.05.

**4.2. Cytotoxicity evaluation using a viability assay**

The cytotoxic activity was assessed using the 3-(4,5-dimethylthiazol-2-yl)-2,5-diphenyl tetrazolium bromide (MTT) colorimetric assay as reported previously [43, 44, 62]. In brief, the tumor cell lines were suspended in medium at concentration  $5 \times 10^4$  cell/well in Corning® 96-well tissue culture plates and then incubated for 24 h. The tested compounds with concentrations ranging from 0 to 50  $\mu\text{g/ml}$  were then added into 96-well plates (six replicates) to achieve different conc. for each compound. Six vehicle controls with media or 0.5 % DMSO were run for each 96 well plate as a control. After incubating for 24 h, the numbers of viable cells were determined by the MTT test. Briefly, the media was removed from the 96 well plates and replaced with 100  $\mu\text{l}$  of fresh culture RPMI 1640 medium without phenol red then 10  $\mu\text{l}$  of the 12 mM MTT stock solution (5 mg of MTT in 1 mL of PBS) to each well including the untreated controls. The 96-well plates were then incubated at 37 oC and 5 % CO<sub>2</sub> for 4 h. An 85- $\mu\text{l}$  aliquot of the media was removed from the wells, and 50  $\mu\text{l}$  of DMSO was added to each well and mixed thoroughly with the pipette and incubated at 37 oC for 10 min. Then, the optical density was measured at 590 nm with the microplate reader (Sunrise, TECAN, Inc, USA) to determine the number of viable cells and the percentage of viability was calculated as  $[1 - (\text{ODt}/\text{ODc})] \times 100 \%$  where ODt is the mean optical density of wells treated with the tested sample and ODc is the mean optical density of untreated cells. The relation between surviving cells and drug concentration is plotted to get the survival curve of each tumor cell line after treatment with the specified compound. The 50 % inhibitory concentration (IC<sub>50</sub>), the concentration required to cause toxic effects in 50 % of intact cells, was estimated from graphic plots of the dose response curve for each conc. using Graph pad Prism software (San Diego, CA, USA).

#### 4.3. EGFR<sup>wild type</sup> assay

EGFR kinase kit was purchased from BPS Bioscience. Briefly, EGFR-ErbB1 (catalog number PV3872), 0.200 mg/mL were used. An ATP solution and a kinase/peptide mixture were prepared right before use. The solutions on the plate were mixed thoroughly, and the plate was incubated for 1 h at room temperature. After that, 5 ml of the developing solution was added to each well. The plate was incubated for 1 h at room temperature and then read by ELISA Reader (PerkinElmer, USA). Curve fitting was performed using Graph Pad Prism. Every experiment was repeated three times. Data represented as means  $\pm$  SD from three independent experiments.

#### 4.4. Quantification of apoptosis by flow cytometry

Annexin V-FITC apoptosis assay was performed by using Annexin V-FITC/PI double staining detection kit (BD Pharmingen, USA).[63, 64] Flow cytometric analysis was performed on FACS Calibur flow cytometer (BD Biosciences, Franklin Lakes, NJ, USA). Annexin V-FITC was detected through (FL1) channel while PI was detected through the (FL2) channel. Finally, a minimum of 10,000 cells per sample were acquired and analyzed using Cell Quest Pro software (BD Biosciences).

#### 4.6. Cell cycle analysis

Cell cycle arrest and distribution was assessed, using the Propidium Iodide Flow Cytometry Kit (ab139418, Abcam) followed by flow cytometry analysis. The DNA content in each cell nucleus was determined by a FACS Calibur flow cytometer (BD Biosciences, Franklin Lakes, NJ, USA). Finally, cell cycle phase distribution was analyzed using Cell Quest Pro software (BD Biosciences) showing collected propidium iodide fluorescence intensity on FL2 [65].

#### Molecular docking

Molecular docking of target compounds into the EGFR protein enzyme comprising the crystal structure of enzyme (PDB ID: 1M17) were retrieved from PDB server (<http://www.pdb.org>) with acceptable resolution using the most active compounds 5a and 5b derivatives. The AutoDock 3.0 [56] and the MOE software [40] were used for all the docking calculations. The detailed protocol was adopted in [39]. The binding energy file generated from docking experiments was used for calculation of the inhibition constants. The protein-ligand interaction plots were generated, using MOE 2012.10. The standard parameter settings were applied. High-scoring binding poses were selected on the basis of visual inspection.

## References

- [1] WHO Report On Cancer, <https://apps.who.int/iris/rest/bitstreams/1267643/retrieve> (2020), pp. 1-160.
- [2] T. Holbro, N.E. Hynes, ErbB receptors: directing key signaling networks throughout life, *Annual review of pharmacology and toxicology*, 44 (2004), pp. 195-217.
- [3] A. Russo, T. Franchina, G.R. Ricciardi, A. Picone, G. Ferraro, M. Zanghi, G. Toscano, A. Giordano, V. Adamo, A decade of EGFR inhibition in EGFR-mutated non small cell lung cancer (NSCLC): Old successes and future perspectives, *Oncotarget*, 6 (2015), pp. 26814-25.
- [4] K.M.M. Alcantara, J. Journal Pre-proofs Redundant and Overlapping Oncogenic Readouts of Non-Canonical and Novel Colorectal Cancer KRAS and NRAS Mutants, *Cells*, 8 (2019), pp. 1557-1579.
- [5] Y.L. Liu, A.M. Horning, B. Lieberman, M. Kim, C.K. Lin, C.N. Hung, C.W. Chou, C.M. Wang, C.L. Lin, N.B. Kirma, M.A. Liss, R. Vasisht, E.P. Perillo, K. Blocher, H. Horng, J.A. Taverna, J. Ruan, T.E. Yankeelov, A.K. Dunn, T.H. Huang, H.C. Yeh, C.L. Chen, Spatial EGFR Dynamics and Metastatic Phenotypes Modulated by Upregulated EphB2 and Src Pathways in Advanced Prostate Cancer, *Cancers*, 11 (2019), pp.
- [6] S. Sebastian, J. Settleman, S.J. Reshkin, A. Azzariti, A. Bellizzi, A. Paradiso, The complexity of targeting EGFR signalling in cancer: from expression to turnover, *Biochimica et biophysica acta*, 1766 (2006), pp. 120-39.
- [7] H.E.A. Ahmed, S.K. Ihmaid, A.M. Omar, A.M. Shehata, H.S. Rateb, M.F. Zayed, S. Ahmed, M.M. Elaasser, Design, synthesis, molecular docking of new lipophilic acetamide derivatives affording potential anticancer and antimicrobial agents, *Bioorganic Chemistry*, 76 (2018), pp. 332-342.
- [8] I.S. Yadav, P.P. Nandekar, S. Srivastava, A. Sangamwar, A. Chaudhury, S.M. Agarwal, Ensemble docking and molecular dynamics identify knoevenagel curcumin derivatives with potent anti-EGFR activity, *Gene*, 539 (2014), pp. 82-90.
- [9] H.-C. Wang, X.-Q. Yan, T.-L. Yan, H.-X. Li, Z.-C. Wang, H.-L. Zhu, Design, Synthesis and Biological Evaluation of Benzohydrazide Derivatives Containing Dihydropyrazoles as Potential EGFR Kinase Inhibitors, *Molecules (Basel, Switzerland)*, 21 (2016), pp. 1012.
- [10] H.-Y. Man, Q. Wang, W.-Y. Lu, W. Ju, G. Ahmadian, L. Liu, S. D'Souza, T.P. Wong, C. Taghibiglou, J. Lu, L.E. Becker, L. Pei, F. Liu, M.P. Wymann, J.F. MacDonald, Y.T. Wang, Activation of PI3-Kinase Is Required for AMPA Receptor Insertion during LTP of mEPSCs in Cultured Hippocampal Neurons, *Neuron*, 38 (2003), pp. 611-624.
- [11] F. Meier, B. Schitteck, S. Busch, C. Garbe, K. Smalley, K. Satyamoorthy, G. Li, M. Herlyn, The RAS/RAF/MEK/ERK and PI3K/AKT signaling pathways present molecular targets for the effective treatment of advanced melanoma, *Frontiers in bioscience : a journal and virtual library*, 10 (2005), pp. 2986-3001.
- [12] M. Sanford, L.J. Scott, Gefitinib: a review of its use in the treatment of locally advanced/metastatic non-small cell lung cancer, *Drugs*, 69 (2009), pp. 2303-28.
- [13] A.M. Soliman, A.S. Alqahtani, M. Ghorab, Novel sulphonamide benzoquinazolinones as dual EGFR/HER2 inhibitors, apoptosis inducers and radiosensitizers, *Journal of enzyme inhibition and medicinal chemistry*, 34 (2019), pp. 1030-1040.
- [14] P. Martins, J. Jesus, S. Santos, L. Raposo, C. Roma-Rodrigues, P. Baptista, A. Fernandes, Heterocyclic Anticancer Compounds: Recent Advances and the Paradigm Shift towards the Use of Nanomedicine's Tool Box, *Molecules*, 20 (2015), pp. 16852.
- [15] H.S. Ibrahim, S.M. Abou-Seri, M. Tanc, M.M. Elaasser, H.A. Abdel-Aziz, C.T. Supuran, Isatin-pyrazole benzenesulfonamide hybrids potently inhibit tumor-associated carbonic anhydrase isoforms IX and XII, *Eur J Med Chem*, 103 (2015), pp. 583-93.
- [16] M.N. Noolvi, H.M. Patel, M. Kaur, Benzothiazoles: Search for anticancer agents, *European Journal of Medicinal Chemistry*, 54 (2012), pp. 447-462.
- [17] B. Aneja, N.S. Khan, P. Khan, A. Queen, A. Hussain, M.T. Rehman, M.F. Alajmi, H.R. El-Seedi, S. Ali, M.I. Hassan, M. Abid, Design and development of Isatin-triazole hydrazones as potential inhibitors of microtubule affinity-regulating kinase 4 for the therapeutic management of cell proliferation and metastasis, *European Journal of Medicinal Chemistry*, 163 (2019), pp. 840-852.
- [18] H.A. Bhuva, S.G. Kini, Synthesis, anticancer activity and docking of some substituted benzothiazoles as tyrosine kinase inhibitors, *Journal of Molecular Graphics and Modelling*, 29 (2010), pp. 32-37.
- [19] C.G. Mortimer, G. Wells, J.P. Crochard, E.L. Stone, T.D. Bradshaw, M.F. Stevens, A.D. Westwell, Antitumor benzothiazoles. 26.(1) 2-(3,4-dimethoxyphenyl)-5-fluorobenzothiazole (GW 610, NSC 721648), a simple fluorinated 2-arylbenzothiazole, shows potent and selective inhibitory activity against lung, colon, and breast cancer cell lines, *J Med Chem*, 49 (2006), pp. 179-85.
- [20] R. Ujan, A. Saeed, P.A. Channar, F.A. Larik, Q. Abbas, M.F. Alajmi, H.R. El-Seedi, M.A. Rind, M. Hassan, H. Raza, S.Y. Seo, Drug-1,3,4-Thiadiazole Conjugates as Novel Mixed-Type Inhibitors of Acetylcholinesterase: Synthesis, Molecular Docking, Pharmacokinetics, and ADMET Evaluation, *Molecules*, 24 (2019), pp. 860-73.
- [21] D. Dheer, V. Singh, R. Shankar, Medicinal Attributes of 1,2,3-Triazoles : Current Developments, *Bioorganic chemistry*, 71 (2017), pp. 30-54.
- [22] P. Martins, J. Jesus, S. Santos, L.R. Raposo, C. Roma-Rodrigues, P.V. Baptista, A.R. Fernandes, Heterocyclic Anticancer Compounds: Recent Advances and the Paradigm Shift towards the Use of Nanomedicine's Tool Box, *Molecules*, 20 (2015), pp. 16852-91.
- [23] M.R. Aouad, M.M. Mayaba, A. Naqvi, S.K. Bardaweel, F.F. Al-Blewi, M. Messali, N. Rezki, Design, synthesis, in silico and in vitro antimicrobial screenings of novel 1,2,4-triazoles carrying 1,2,3-triazole scaffold with lipophilic side chain tether, *Chemistry Central journal*, 11 (2017), pp. 117.
- [24] N. Rezki, Green Microwave Synthesis and Antimicrobial Evaluation of Novel Triazoles, *Organic Preparations and Procedures International*, 49 (2017), pp. 525-541.
- [25] N. Rezki, M.R. Aouad, Green ultrasound-assisted three-component click synthesis of novel 1H-1,2,3-triazole carrying benzothiazoles and fluorinated-1,2,4-triazole conjugates and their antimicrobial evaluation, *Acta pharmaceutica (Zagreb, Croatia)*, 67 (2017), pp. 309-324.
- [26] N. Rezki, M.M. Mayaba, F.F. Al-blewi, M.R. Aouad, E.S.H. El Ashry, Click 1,4-regioselective synthesis, characterization, and antimicrobial screening of novel 1,2,3-triazoles tethering fluorinated 1,2,4-triazole and lipophilic side chain, *Research on Chemical Intermediates*, 43 (2017), pp. 995-1011.
- [27] F.F. Al-Blewi, M.A. Almeahadi, M.R. Aouad, S.K. Bardaweel, P.K. Sahu, M. Messali, N. Rezki, E.S.H. El Ashry, Design, synthesis, ADME prediction and pharmacological evaluation of novel benzimidazole-1,2,3-triazole-sulfonamide hybrids as antimicrobial and antiproliferative agents, *Chemistry Central journal*, 12 (2018), pp. 110-110.
- [28] Z. Xu, S.-J. Zhao, Y. Liu, 1,2,3-Triazole-containing hybrids as potential anticancer agents: Current developments, action mechanisms and structure-activity relationships, *European Journal of Medicinal Chemistry*, 183 (2019), pp. 111700.
- [29] I.E. Valverde, A. Bauman, C.A. Kluba, S. Vomstein, M.A. Walter, T.L. Mindt, 1,2,3-Triazoles as amide bond mimics: triazole scan yields protease-resistant peptidomimetics for tumor targeting, *Angewandte Chemie (International ed. in English)*, 52 (2013), pp. 8957-60.
- [30] I.E. Valverde, T.L. Mindt, 1,2,3-Triazoles as amide-bond surrogates in peptidomimetics, *Chimia*, 67 (2013), pp. 262-6.
- [31] N.M. Grob, S. Schmid, R. Schibli, M. Behe, T.L. Mindt, Design of Radiolabeled Analogs of Minigastrin by Multiple Amide-to-Triazole Substitutions, *Journal of Medicinal Chemistry*, (2020), pp.
- [32] R.M. Kumbhare, U.B. Kosurkar, M. Janaki Ramaiah, T.L. Dadmal, S.N.C.V.L. Pushpavalli, M. Pal-Bhadra, Synthesis and biological evaluation of novel triazoles and isoxazoles linked 2-phenyl benzothiazole as potential anticancer agents, *Bioorganic & medicinal chemistry letters*, 22 (2012), pp. 5424-5427.
- [33] M.R. Aouad, M.A. Almeahadi, N. Rezki, F.F. Al-blewi, M. Messali, I. Ali, Design, click synthesis, anticancer screening and docking studies of novel benzothiazole-1,2,3-triazoles appended with some bioactive benzofused heterocycles, *Journal of Molecular Structure*, 1188 (2019), pp. 153-164.
- [34] M.R. Aouad, M.A. Soliman, M.O. Alharbi, S.K. Bardaweel, P.K. Sahu, A.A. Ali, M. Messali, N. Rezki, Y.A. Al-Soud, Design, Synthesis and Anticancer Screening of Novel Benzothiazole-Piperazine-1,2,3-Triazole Hybrids, *Molecules (Basel, Switzerland)*, 23 (2018), pp.
- [35] N. Rezki, A Green Ultrasound Synthesis, Characterization and Antibacterial Evaluation of 1,4-Disubstituted 1,2,3-Triazoles Tethering Bioactive Benzothiazole Nucleus, *Molecules (Basel, Switzerland)*, 21 (2016), pp. 505.

- [36] F. Grisoni, D. Merk, R. Byrne, G. Schneider, Scaffold-Hopping from Synthetic Drugs by Holistic Molecular Representation, *Scientific reports*, 8 (2018), pp. 16469-16469.
- [37] X. Deng, X. Tan, T. An, Q. Ma, Z. Jin, C. Wang, Q. Meng, C. Hu, Synthesis, Characterization, and Biological Activity of a Novel Series of Benzo[4,5]imidazo[2,1-b]thiazole Derivatives as Potential Epidermal Growth Factor Receptor Inhibitors, *Molecules* (Basel, Switzerland), 24 (2019), pp. 682.
- [38] İ. Celik, G. Ayhan-Kılıçgil, B. Guven, Z. Kara, A.S. Gurkan-Alp, A. Karayel, A. Onay-Besikci, Design, synthesis and docking studies of benzimidazole derivatives as potential EGFR inhibitors, *European Journal of Medicinal Chemistry*, 173 (2019), pp. 240-249.
- [39] H.E.A. Ahmed, S.K. Ihmaid, A.M. Omar, A.M. Shehata, H.S. Rateb, M.F. Zayed, S. Ahmed, M.M. Elaasser, Design, synthesis, molecular docking of new lipophilic acetamide derivatives affording potential anticancer and antimicrobial agents, *Bioorganic chemistry*, 76 (2018), pp. 332-342.
- [40] M. Molecular Operating Environment (MOE) Chemical Computing Group, Quebec, Canada. 2012; <http://www.chemcomp.com>. Accessed on 30/02/2013, pp.
- [41] N. Batra, V. Rajendran, D. Agarwal, I. Wadi, P.C. Ghosh, R.D. Gupta, M. Nath, Synthesis and Antimalarial Evaluation of [1, 2,3]-Triazole-Tethered Sulfonamide-Berberine Hybrids, *ChemistrySelect*, 3 (2018), pp. 9790-9793.
- [42] P.D. Leeson, B. Springthorpe, The influence of drug-like concepts on decision making in medicinal chemistry, *Nature Reviews Drug Discovery*, 6 (2007), pp. 881-890.
- [43] T. Mosmann, Rapid colorimetric assay for cellular growth and survival: application to proliferation and cytotoxicity assays, *Journal of immunological methods*, 65 (1983), pp. 55-63.
- [44] F. Demirci, K.H.C. Başer, *Bioassay Techniques for Drug Development* By Atta-ur-Rahman, M. Iqbal Choudhary (HEJRIC, University of Karachi, Pakistan), William J. Thomsen (Areana Pharmaceuticals, San Diego, CA). Harwood Academic Publishers, Amsterdam, The Netherlands. 2001. xii + 223 pp., *Journal of Natural Products*, 65 (2002), pp. 1086-1087.
- [45] S.Y. Proskuryakov, V.L. Gabai, Mechanisms of tumor cell necrosis, *Current pharmaceutical design*, 16 (2010), pp. 56-68.
- [46] J.M. Coppola, B.D. Ross, A. Rehemtulla, Noninvasive imaging of apoptosis and its application in cancer therapeutics, *Clinical cancer research : an official journal of the American Association for Cancer Research*, 14 (2008), pp. 2492-501.
- [47] S. Liu, H. Cao, D. Chen, S. Yu, H. Sha, J. Wu, R. Ma, Z. Wang, C. Jing, J. Zhang, J. Feng, LXR ligands induce apoptosis of EGFR-TKI-resistant human lung cancer cells in vitro by inhibiting Akt-NF-κB activation, *Oncol Lett*, 15 (2018), pp. 7168-7174.
- [48] S. Ali, S. Banerjee, A. Ahmad, B.F. El-Rayes, P.A. Philip, F.H. Sarkar, Apoptosis-inducing effect of erlotinib is potentiated by 3,3'-diindolylmethane in vitro and in vivo using an orthotopic model of pancreatic cancer, *Mol Cancer Ther*, 7 (2008), pp. 1708-1719.
- [49] A. Huether, M. Hopfner, A.P. Sutter, D. Schuppan, H. Scherubl, Erlotinib induces cell cycle arrest and apoptosis in hepatocellular cancer cells and enhances chemosensitivity towards cytostatics, *Journal of hepatology*, 43 (2005), pp. 661-9.
- [50] T.I. de Santana, M.d.O. Barbosa, P.A.T.d.M. Gomes, A.C.N. da Cruz, T.G. da Silva, A.C.L. Leite, Synthesis, anticancer activity and mechanism of action of new thiazole derivatives, *European journal of medicinal chemistry*, 144 (2018), pp. 874-886.
- [51] G. Chandrasekaran, P. Tátrai, F. Gergely, Hitting the brakes: targeting microtubule motors in cancer, *Br J Cancer*, 113 (2015), pp. 693-698.
- [52] P.R. Dutta, A. Maity, Cellular responses to EGFR inhibitors and their relevance to cancer therapy, *Cancer Lett*, 254 (2007), pp. 165-177.
- [53] A.E. Quatrala, L. Porcellini, N. Silvestris, G. Colucci, A. Angelo, A. Azzariti, EGFR tyrosine kinases inhibitors in cancer treatment: in vitro and in vivo evidence, *Frontiers in bioscience (Landmark edition)*, 16 (2011), pp. 1962-72.
- [54] S. Ihmaid, H.E.A. Ahmed, M.F. Zayed, The Design and Development of Potent Small Molecules as Anticancer Agents Targeting EGFR TK and Tubulin Polymerization, *International journal of molecular sciences*, 19 (2018), pp.
- [55] M. Alswah, A.H. Bayoumi, K. Elgamal, A. Elmorsy, S. Ihmaid, H.E.A. Ahmed, Design, Synthesis and Cytotoxic Evaluation of Novel Chalcone Derivatives Bearing Triazolo[4,3-a]-quinoxaline Moieties as Potent Anticancer Agents with Dual EGFR Kinase and Tubulin Polymerization Inhibitory Effects, *Molecules* (Basel, Switzerland), 23 (2017), pp.
- [56] G.M. Morris, D.S. Goodsell, R.S. Halliday, R. Huey, W.E. Hart, R.K. Belew, A.J. Olson, Automated docking using a Lamarckian genetic algorithm and an empirical binding free energy function, *Journal of computational chemistry*, 19 (1998), pp. 1639-1662.
- [57] H.M. Berman, J. Westbrook, Z. Feng, G. Gilliland, T.N. Bhat, H. Weissig, I.N. Shindyalov, P.E. Bourne, The Protein Data Bank, *Nucleic acids research*, 28 (2000), pp. 235-42.
- [58] J. Stamos, M.X. Sliwkowski, C. Eigenbrot, Structure of the epidermal growth factor receptor kinase domain alone and in complex with a 4-anilinoquinazoline inhibitor, *The Journal of biological chemistry*, 277 (2002), pp. 46265-72.
- [59] K. Arnold, L. Bordoli, J. Kopp, T. Schwede, The SWISS-MODEL workspace: a web-based environment for protein structure homology modelling, *Bioinformatics* (Oxford, England), 22 (2006), pp. 195-201.
- [60] D.E. Pires, D.B. Ascher, CSM-lig: a web server for assessing and comparing protein-small molecule affinities, *Nucleic acids research*, 44 (2016), pp. W557-61.
- [61] D.E. Pires, T.L. Blundell, D.B. Ascher, pkCSM: Predicting Small-Molecule Pharmacokinetic and Toxicity Properties Using Graph-Based Signatures, *J Med Chem*, 58 (2015), pp. 4066-72.
- [62] A.M. Omar, J. Bajorath, S. Ihmaid, H.M. Mohamed, A.M. El-Agrody, A. Mora, M.E. El-Araby, H.E.A. Ahmed, Novel molecular discovery of promising amidine-based thiazole analogues as potent dual Matrix Metalloproteinase-2 and 9 inhibitors: Anticancer activity data with prominent cell cycle Arrest and DNA fragmentation analysis effects, *Bioorganic Chemistry*, (2020), pp. 103992.
- [63] M. van Engeland, L.J. Nieland, F.C. Ramaekers, B. Schutte, C.P. Reutelingsperger, Annexin V-affinity assay: a review on an apoptosis detection system based on phosphatidylserine exposure, *Cytometry*, 31 (1998), pp. 1-9.
- [64] I. Vermes, C. Haanen, H. Steffens-Nakken, C. Reutelingsperger, A novel assay for apoptosis. Flow cytometric detection of phosphatidylserine expression on early apoptotic cells using fluorescein labelled Annexin V, *Journal of immunological methods*, 184 (1995), pp. 39-51.
- [65] M. Rosner, K. Schipany, M. Hengstschlager, Merging high-quality biochemical fractionation with a refined flow cytometry approach to monitor nucleocytoplasmic protein expression throughout the unperturbed mammalian cell cycle, *Nature protocols*, 8 (2013), pp. 602-26.

#### Highlights

1. Introducing of 1,2,3-Triazole-based scaffold for design of EGFR inhibitors.
2. Anticancer screening of novel analogues against a panel of cancer cell lines.
3. Molecular docking analyses was done for SAR interpretation.
4. ADMET studies were done for most active derivatives.